

DISSERTATION
submitted
to the
Combined Faculty for the Natural Sciences and Mathematics
of the
Heidelberg University, Germany
for the degree of
Doctor of Natural Sciences

Put forward by
Dipl. Inf. Alena Bakulina
Born in Minsk, Belarus

Automated ultrasound calibration solution for the Ultrasound Fracture Analysis Scanning System

Advisor: Prof. Dr. Reinhard Männer
Second advisor: Prof. Dr. Jürgen Hesser

Abstract

Ultrasound calibration is an essential element for morphometric three-dimensional (3D) ultrasound medical systems that are equipped with two-dimensional (2D) ultrasound probes (transducers). Such systems have a position sensor that measures the position of a transducer in space. These measurements are used to combine 2D ultrasound scans into a 3D volume for further object reconstruction and visualisation. However, spatial transformation between the scan coordinate system and the position sensor transmitter remains unknown. The calibration procedure provides this transformation, normally obtained by scanning a device with known geometrical properties called ultrasound phantom. The accuracy of the calibration transformation directly influences the 3D reconstruction quality, however the accuracy is not the only quality characteristic of a calibration device. Phantoms vary in construction providing different calibration procedures, speed, number and positions of scans, type of calibration landmarks, automatic or manual data acquisition and segmentation, and many other criteria. The calibration method should be chosen individually for every calibrated system and there is no "one for all" solution.

In this work we introduce a novel calibration phantom with a custom calibration procedure designed for the UFASS – the Ultrasound Fracture Analysis Scanning System – an automated scanner for orthopaedic diagnostics. Our method is designed to fulfil the calibration objectives of the UFASS which are not fully covered by any of the standard phantoms.

Our phantom is based on spherical landmarks chosen for their support of a number of calibration requirements such as automated data acquisition and segmentation, and a variety of scanning positions and orientations. It consists of 12 small balls that centre coordinates must be measured with the ultrasound probe during the calibration procedure. We suggest and successfully implement a novel method to obtain and process the input ultrasound data from the phantom without manual operations from a user. Our method uses the motion controller of the UFASS to sequentially move the ultrasound probe and obtain parallel sphere slices with a small step. The scan corresponding to the central section is found by matching a circle template of the sphere's radius to each image. The image with the highest cross-correlation with the template is the central sphere section and its circle centre is the sphere's centre.

For the UFASS our method outperforms comparable calibration solutions providing the automated data acquisition and landmarks detection procedure, high calibration speed, low calibration error, and requiring no experience and no expert knowledge from the end user performing the calibration.

Zusammenfassung

Für morphometrische, dreidimensionale, medizinische Ultraschallsysteme, die mit zweidimensionalen Ultraschallköpfen (Transducern) ausgerüstet sind, ist die Ultraschallkalibrierung ein wesentlicher Bestandteil. Solche Systeme haben einen Positionssensor um die Position des Transducers im Raum zu messen. Diese Messungen werden gebraucht um 2D Ultraschallbilder in ein 3D Volumen zu vereinen um weitere Objekt Rekonstruktionen und Visualisierungen zu ermöglichen. Die geometrische Transformation zwischen dem Koordinatensystem des Bildes und dem Positionssensortransmitter ist jedoch unbekannt. Die Ultraschallkalibrierung liefert diese Transformation, welche normalerweise beim Scannen eines Objektes mit bekannten geometrischen Proportionen erhalten wird. So ein Objekt wird ein Ultraschallphantom genannt. Die Genauigkeit von der Ultraschallkalibrierung beeinflusst direkt die Qualität der Objektrekonstruktion, allerdings ist die Genauigkeit nicht das einzige Maß für die Ultraschallphantomqualität. Phantome variieren in ihrer Beschaffenheit und verfügen über verschiedene Eigenschaften: Kalibrierungsverfahren, Geschwindigkeit der Kalibrierung, benötigte Quantität von Ultraschallbildern, Typen von Kalibrierungsmarkern (auch Landmarkern genannt), automatische oder manuelle Datenaufnahme und Segmentierung, und viele weitere Kriterien. Die Kalibrierungsmethode muss individuell für jedes System ausgewählt werden, da es nicht die eine "Lösung für alle Fälle" gibt.

In dieser Arbeit präsentieren wir ein neues Kalibrierungsphantom mit einem eigenen Kalibrierungsverfahren, welches speziell für den UFASS – den Ultraschall Scanner für Knochenbruch Diagnostik – konzipiert wurde. Unsere Methode deckt die Kalibrierungsziele des Ultrasound Fracture Analysis Scanning System (UFASS) ab, die von den anderen standardmäßigen Kalibrierungsverfahren nicht abgedeckt werden.

Unser Phantom ist auf kugelförmigen Landmarken basiert, die gewählt wurden um möglichst viele Kalibrierungsanforderungen zu unterstützen, z.B. automatische Datenaufnahme und Segmentierung und eine Vielfalt von Scanpositionen und Ausrichtungen. Das Phantom besteht aus 12 kleinen Kugeln, deren Zentren mit Hilfe des Ultraschallkopfes während des Kalibrierungsvorganges gemessen werden müssen. Wir haben erfolgreich eine Methode entwickelt und implementiert, welche diese Ultraschallbilder automatisch aufnimmt und verarbeitet ohne ein manuelles Eingreifen des Systemnutzers zu benötigen. Unsere Methode benutzt den Bewegungskontroller des UFASS für sequenzielle Bewegungen des Ultraschallkopfes und erhält so parallele Kugelschnitten mit gleicher, kleiner Schrittweite. Das Ultraschallbild, das dem zentralen Schnitt der Kugel entspricht, wird gefunden, in dem man ein Kreistempalte des Kugelradius auf jedes Bild anpasst. Das Bild mit dem größten Kreuzkorrelationswert mit dem Template ist der Schnitt durch das Zentrum der Kugel und sein Kreiszentrum ist das Kugelzentrum.

Für den UFASS übertrifft unsere Methode die vergleichbaren State-of-the-Art

Kalibrierungsmethoden und verfügt über eine automatische Datenaufnahme und Segmentierung, eine hohe Kalibrierungsgeschwindigkeit und kleine Kalibrierungsfehler. Das Verfahren erfordert keine spezielle Erfahrung oder Expertenwissen des Systemnutzers um die Kalibrierung auf unsere Weise durchzuführen.

Contents

Notation	13
List of Figures	15
List of Tables	17
Introduction	19
1 Ultrasound calibration	23
1.1 Ultrasound image modality	23
1.2 Ultrasound calibration task	24
1.3 Ultrasound calibration phantoms	26
1.3.1 Point phantoms	26
1.3.1.1 Cross-wire phantom	27
1.3.1.2 Spherical landmarks	28
1.3.1.3 Stylus	29
1.3.2 Wire phantoms	30
1.3.2.1 Three-wire phantom	30
1.3.2.2 Z-phantom	31
1.3.2.3 Other wire phantoms	32
1.3.3 Plane phantoms	32
1.3.3.1 Single-wall phantom	33
1.3.3.2 Cambridge phantom	34
1.3.3.3 Plane phantom with wires	35
1.3.4 Alignment phantoms	35
1.3.4.1 Shaped board	36

1.3.4.2	Mechanical instrument	36
1.3.4.3	Planar strings array	37
1.3.4.4	Wedges phantom	38
1.3.5	Registration phantoms	39
2	Ultrasound Fracture Analysis Scanning System	41
2.1	Automated ultrasound systems	41
2.2	UFASS	43
2.2.1	Design and application	43
2.2.2	Prototype	44
2.3	UFASS calibration requirements	46
2.4	Analysis of existing calibration techniques in application to UFASS calibration	48
2.4.1	Point phantoms	49
2.4.2	Wire phantoms	49
2.4.3	Plane phantoms	50
2.4.4	Alignment phantoms	50
2.4.5	Registration phantoms	51
2.4.6	Other phantoms	51
2.4.7	Resume	52
3	The multi-spheres phantom for the UFASS calibration	55
3.1	The multi-spheres phantom	55
3.1.1	Landmark	56
3.1.1.1	Choosing landmark material and size	56
3.1.1.2	Ball's centre detection in a series of sequential par- allel ultrasound (US) slices	57
3.1.1.3	Ball's centre detection in a series of sequential an- gular US slices	59
3.1.1.4	Ball's centre detection accuracy	66
3.1.2	Choosing phantom geometry	67
3.1.3	Phantom design	70
3.1.4	Phantom model	71
3.1.5	Scanner calibration	71
3.1.6	Application to other automatic scanners	75

Contents

3.2	Results	75
3.2.1	Alternative calibration with the multi-wires phantom . . .	80
3.3	Discussion	82
	Conclusion	85
	Appendix A. Spatial localizer	87
	Appendix B. Calibration software	91
	Bibliography	94
	Acknowledgements	103

Notation

2D	two-dimensional
3D	three-dimensional
US	ultrasound
B-scan	2D ultrasound image
DOF	degrees of freedom
CT	computer tomography
MRI	magnetic resonance imaging
RMS	root mean square
UFASS	Ultrasound Fracture Analysis Scanning System
UON	UltraOsteon GmbH

List of Figures

1.1	Calibration coordinate systems: US image (I), position sensor's mobile part (P), position sensor's stationary counterpart (S), global (G) coordinate systems.	25
1.2	Cross-wire phantom.	27
1.3	Stylus for passive optical tracking from <i>Northern Digital Inc.</i>	29
1.4	Three-wire phantom.	30
1.5	Z-phantom.	31
1.6	Single-wall phantom.	33
1.7	Beam width problem.	34
1.8	Cambridge phantom (Prager et al. [73]).	34
1.9	Hybrid plane-wire phantom.	35
1.10	Sato et al. shaped board alignment phantom.	36
1.11	Other shaped board alignment phantoms.	37
1.12	Gee et al. mechanical instrument.	38
1.13	Leotta alignment phantom.	39
2.1	<i>OTELLO</i> tele-echography system [66].	42
2.2	An ultrasound tomography system [34].	43
2.3	UFASS model (©UltraOsteon GmbH).	45
2.4	UFASS prototype.	45
3.1	Balls for the landmark material and size selection test.	57
3.2	Circles detection on the B-scans.	61
3.3	Standard B-scan for the chosen plastic balls.	62
3.4	Ball's centre detection with unknown diameter.	62

3.5	US beam trajectory for a transducer rotated around the ball's axis. 3.5a: An US beam can pass not directly through a ball's centre. 3.5b: An error ε of centre location with the beam angular deflection of $\alpha/2$ and the R distance from the transducer to the ball's centre.	63
3.6	Centre detection error for a transducer rotated around the ball's axis. A surface shows the error value ε depending on the rotation angle step α (in degrees) and the distance R (in mm) from the transducer to the ball's centre.	63
3.7	Centre detection error for a transducer rotated around the ball's axis. Each spiral curve shows the error value ε depending on the rotation angle step α (in degrees, each α value corresponds to one circle) for a fixed distance R (in mm) from the transducer to the ball's centre. A red circle represents the error threshold (0.2 mm) which is selected as the highest acceptable value for this experiment. Straight coloured lines correspondent to each curve show the α value at which this threshold is achieved for the fixed R value. Each values pair (α, R) inside the red circle is permitted for the experiment.	64
3.8	Ball's centre detection from a series of images. A known-size object with a ball on it gives a B-scan on which both the ball's circle section and the metal surface under the ball can be detected. . . .	66
3.9	Possible phantom configurations. First model has higher variety of angles ($0^\circ, 36^\circ, 72^\circ, 108^\circ, 144^\circ, 180^\circ, 216^\circ, 252^\circ, 288^\circ, 324^\circ$), one ball at each height. Second model has two balls at each height, fewer height levels at four angles ($0^\circ, 90^\circ, 180^\circ, 270^\circ$). Third model has one ball per height level at four angles ($0^\circ, 90^\circ, 180^\circ, 270^\circ$). . .	68
3.10	The multi-spheres phantom.	70
3.11	Multi-spheres phantom data acquisition for parallel and angular scanning procedure.	74
3.12	Multi-spheres phantom in the UFASS calibration.	76
3.13	Multi-wires phantom.	81
3.14	MicroScribe 3D digitizer ([63]).	88
3.15	MicroScribe digitizer measurements precision.	89
3.16	An example of the configuration file for the multi-spheres phantom calibration software.	91

List of Tables

2.1	Fulfilment of the UFASS calibration objectives by standard calibration phantoms.	53
3.1	Error of centre detection for a transducer rotated around the ball's axis, depending on the scanning angle step. Cells marked with gray correspond to the value pair (α, R) which are acceptable for the experiment assuming the error threshold equal to 0.2 mm.	65
3.2	Phantom Model 1 simulation. Calibration error depending on the ball's quantity and maximal value of the random error in the calibration data.	69
3.3	Phantom Model 2 simulation. Calibration error depending on the ball's quantity and maximal value of the random error in the calibration data.	69
3.4	Phantom Model 3 simulation. Calibration error depending on the ball's quantity and maximal value of the random error in the calibration data.	69
3.5	UFASS calibration root mean square (RMS) error (in mm) with the multi-spheres phantom.	77
3.6	Fulfilment of the UFASS calibration objectives by the multi-spheres and the multi-wires calibration phantoms.	80
3.7	MicroScribe spatial localizer measurements precision. Coordinates (in mm) variance is given for each of the three experiments.	88

Introduction

Ultrasound is a very popular image modality in medical diagnostics. Though the freehand ultrasound is still the most widely used in medical practice, there is a big variety of automated ultrasound scanners that provide more complex diagnostics including reconstruction and visualisation of a scanned object in the 3D space. Such systems are extremely useful in cardiology, orthopaedics, cancer diagnostics, and other applications with the importance of volumetric information analysis of the scanned object. For this purpose either a two-dimensional or a three-dimensional ultrasound transducer (also frequently called an ultrasound probe) can be used. When a system is equipped with a 3D transducer we directly obtain volumetric information from the transducer's data. However, 3D transducers have several known disadvantages, e.g. lower resolution, higher costs, larger probe size that may be inappropriate for some surfaces [61]. Thereby 2D ultrasound probes are often used in 3D applications. In these systems obtained 2D ultrasound images are assembled into a 3D volume using additional position data of the images in the 3D space. To get this data the common approach is to equip the system with a position sensor that tracks the movements of an ultrasound probe [73, 61, 41]. The sensor tracks spatial movements of the probe with respect to the sensor's stationary counterpart or to some fixed coordinate system. There are several classes of position sensors – optical, electromagnetical, mechanical [22, 62]. However, independently of the sensor type, in any ultrasound system there is one unknown parameter – the position and orientation of an ultrasound (US) image with respect to the tracking part of the position sensor. This unknown parameter is described by a transformation matrix from the US image coordinate system to the tracking coordinate system. The process of obtaining this transformation is called ultrasound calibration and the transformation itself is called calibration matrix. The calibration matrix is later used in the reconstruction of the 3D volume, therefore it greatly influences the resulting system's accuracy. To obtain the calibration matrix for a 3D ultrasound system a standard approach is to scan a special object with known geometrical properties called "phantom" [41, 61].

In this work we present the calibration solution for the UFASS automated ultrasound system – the Ultrasound Fracture Analysis Scanning System. It is a medical ultrasound scanner for diagnostics of extremities fractures in or-

thopaedics. It is designed as an alternative to computer tomography in order to reduce the radiation dose for the patient. The UFASS can substitute computer tomography (CT) in several cases, which is very practical for sensitive patients such as children and pregnant women [14]. It is a compact non-invasive medical device with a simple investigation principle. Its main part consists of two ultrasound transducers and a water tank with a fixation system for the extremity. The transducers are oriented in the direction of the tank centre and may be rotated around it and elevated in the vertical direction. This way their motion trajectories cover the extremity from all positions and orientations and allow to build a full 3D model of it. The transducers are moved automatically, operated by a position controller. For each investigation a new water tank for each patient is used, wherefore the transducers are reattached and attached back each time. Therefore the system must be often calibrated because even minimal displacement of the transducer may cause a big error in the final data reconstruction. This application demands for several requirements to the calibration phantom and procedure, such as robustness, low costs and construction simplicity, execution simplicity and speed (a fast calibration procedure), self-sufficiency and expert-independence (no extra equipment and/or personnel with calibration experience involved), distances range support (phantom landmarks are well recognized on different distances to the transducer), positions and orientations variety support, and automated image processing. The construction of the scanner also requires the phantom to be detectable from all possible transducer positions, which is important to provide good accuracy along the whole motion curve of the US probe. And the main requirement to the system is a fully-automated landmarks detection, since manual image segmentation is the main source of non-repeatability of the calibration, requires an expert to perform it, and takes a lot of time.

Calibration phantoms can be classified according to the type of their landmarks – the scanned phantom parts that produce an ultrasound response. This response is detected from the US scan and is used to determine the position of the phantom in space. First calibration phantoms used simple point landmarks, such as a bead or a top of a stylus [7, 8, 53, 55, 67, 81, 89]. Though the construction of such phantom was very simple, the calibration took a lot of time and required an experienced professional to perform it. The main disadvantage of these methods was the necessity to manually align the ultrasound probe with the point and further detect the point on the image. Due to the properties of the ultrasound beam both tasks were not trivial. An improvement that simplified the alignment step was a cross-wire phantom, which landmark was a crossing of two wires [5, 9, 27, 43, 60, 83]. However data acquisition and segmentation still remained complicated, and the next idea was to use a wire section as a landmark, because it required no alignment since every point of a wire could be accepted as an input landmark [19, 73, 41]. The alignment problem was solved, but manual segmentation was anyway required because the landmark was still presented as

a single point on an ultrasound scan. Moreover, a new problem appeared – the proposed wire-based calibration solution required very precise construction and measurements that influenced the result accuracy. The novel idea to use a plane as a landmark, firstly presented as a single wall phantom, ought to solve both data acquisition and segmentation problems [10, 51, 65, 73, 74]. A plane scanned with an ultrasound probe appeared as a line on the ultrasound image. This line could be detected automatically. But it was stated that due to the beam width problem the phantom could be scanned only from the direction orthogonal to the scanning plane, otherwise the accuracy of the calibration was very low. The improvement of the plane phantom idea was a Cambridge phantom [3, 72, 84] that provided a special phantom-holding clamp that fixed the beam-width problem. The disadvantage of this phantom was its complexity and price, moreover it required to attach the transducer to the clamp, that made it applicable only for the freehand ultrasound, but not for the automated scanners. The other idea to reduce the calibration complexity and time was not to automate the calibration procedure, but to reduce the amount of data processed for the calibration, that resulted in alignment phantoms [12, 54, 78, 87]. They normally required only one scan since they had a configuration with several landmarks that uniquely defined the phantom position. Unfortunately aligning the scanning plane with all landmarks at once remained a time-consuming and expert-dependent task. As a variation of this idea one very accurate and relatively easy in use phantom – the mechanical instrument – was proposed [33], but as well as the Cambridge phantom it was only suitable for freehand ultrasound calibration, and its price and construction complexity were very high. The last class of ultrasound phantoms implemented an independent idea – the data registration. As a registration phantom some device with unique morphology was selected and scanned using ultrasound and some another image modality, like computer tomography or magnetic resonance imaging [13, 44, 52, 69]. The calibration matrix was obtained by matching two datasets to each other. The disadvantage of this phantom was its low accuracy in comparison to the other phantom classes.

The detailed description of each phantom class is given in the Chapter 1. Though there are many standard calibration phantoms presented in the literature, they all have disadvantages. Each medical system has its one calibration requirements with focus on different objectives, such as speed, automation, high accuracy, repeatability, and many others, and no phantom satisfies all of the objectives at once [61, 72]. Moreover, the majority of the state of the art calibration phantoms are better applicable for the freehand ultrasound systems, whereas for the automated scanners the known calibration solutions must be adjusted or designed individually. To choose the right calibration phantom and procedure for an ultrasound system one must firstly analyse the system's calibration objectives and find the appropriate trade-off between the drawbacks and required features. Analysis of the known calibration phantoms in application to the UFASS calibra-

tion objectives shows that there is no proper ready solution for the UFASS. The main UFASS requirement is the automatic image data segmentation. Phantoms providing this property are not applicable either because they are developed only for the freehand ultrasound and require attaching the US probe to the phantom (Cambridge phantom and the Mechanical instrument), or do not support the visibility from both UFASS transducers (Z-phantom). Other phantom types also suffer from lack of calibration requirements support for our system, such as variety of positions and orientation, easiness of data acquisition, expert-independence, etc. We provide a detailed report analysing each type of standard calibration phantoms in application to the UFASS calibration requirements that proves this statement. The UFASS manufacturer provides it's own multi-wires calibration phantom that better suits the calibration goals as the state of the art phantoms, however it does not satisfy all of the calibration objectives as well.

The goal of this work is to design a new calibration phantom with a custom calibration procedure for the calibration of the UFASS that outperforms the standard and the multi-wires phantoms in application to the UFASS and implements all of the scanner's calibration objectives. We achieve this goal with a novel multi-spheres phantom based on spherical landmarks that are very practical for automatic detection and image segmentation. For this phantom we design a new fully-automatic procedure for data acquisition that is a know-how in comparison to the standard calibration techniques where the ultrasound data is obtained manually. Usage of the UFASS's position controller enables to automate this calibration step.

Structure of the work

This work is organized as follows. Firstly, we give a definition of the 2D ultrasound calibration task and propose a detailed overview of existing calibration phantoms in the chapter 1. In the second chapter we introduce the UFASS and state its calibration requirements. There we provide the full analysis of existing calibration phantoms in application to the stated calibration objectives and formulate requirements to an ideal calibration phantom for the UFASS. Then, in the third chapter, we present our calibration phantom, describe the designed calibration procedure and automatic landmarks detection method in details. We also compare our calibration phantom to the multi-wires phantom. Finally we discuss the method advantages and disadvantages using the performed calibration experiments results.

Chapter 1

Ultrasound calibration

1.1 Ultrasound image modality

Ultrasound image modality is very popular in medical diagnostics already several decades. An image is obtained using a transducer made of beam emitter/receiver elements that transmit ultrasound pulses into the body and receive the response echoes that are reflected or scattered back from the body organs. Each element is typically a piezoelectric crystal that transforms an electric impulse into the ultrasound wave and back. Depending on the number and positioning of the emitters/receivers there are one-dimensional, two-dimensional and three-dimensional transducers. For each type of transducer the resulting grayscale image is a function of the magnitude and the response time of these echoes. The B-mode (brightness mode) resulting in a B-scan is one of the most commonly used ultrasound image modes nowadays. A 1D transducer has only one piezoelement that gives a one-dimensional array back, 2D consists of a linear array of elements giving a two-dimensional image back, and the 3D transducer has a matrix of emitters/receivers that produce a 3D data volume.

Ultrasound has a number of advantages over other medical image modalities, e.g. the low costs, portability, safety for the patient, and high image resolution. However, due to the physical properties of sound wave propagation in tissues the quality of the images is not very high, they are often bulky and prone to artifacts. It makes ultrasound images not an easy target for object detection and segmentation.

The most conventional ultrasound is the 2D that is intensively being used since the 1960th, where it was first presented by Siemens. In the last two decades the 3D transducers are also being actively developed, but they still suffer from poor image quality, a lot of artifacts and insufficient image coverage, therefore they are mostly used just in several applications, like scanning a heart [45]. The main advantage of the 3D ultrasound in comparison to the 2D is that it directly

provides the volumetric image data. However, due to the named disadvantages, using 2D ultrasound in combination with a position sensor arranging 2D scans into a 3D space often gives a better result.

1.2 Ultrasound calibration task

Spatial ultrasound system calibration (referred as ultrasound calibration) is required to correctly organise 2D ultrasound images into a 3D volume. This task takes place in the ultrasound systems that are equipped with 2D transducers and a position sensor that tracks the position of the transducer in the 3D space. The calibration then is a process of obtaining a fixed transformation between the ultrasound image coordinate system and the position sensor's transmitter part (it's mobile part that is attached to the transducer and moved with it).

The ultrasound calibration process involves several coordinate systems illustrated on the Figure 1.1. I is the US image coordinate system, where X -axis is the lateral direction, Y -axis in the beam propagation direction and Z -axis is orthogonal to the image plane. P and S are position sensor's mobile part and its stationary counterpart coordinate systems respectively. Under the position sensor's coordinate system its mobile part's system is often meant. G is the global coordinate system. Global coordinate system is the system where the final object volume is constructed in the 3D space. System G can be sometimes combined with the calibration phantom coordinate system.

The full transformation that converts a point on an US image to a point in the global coordinate system is represented by the equation (1.1):

$$p_G = T_{G \leftarrow S} \cdot T_{S \leftarrow P} \cdot T_{P \leftarrow I} \cdot p_I \quad (1.1)$$

$$p_I = \begin{pmatrix} s_x \cdot u \\ s_y \cdot v \\ 0 \\ 1 \end{pmatrix}, \quad p_G = \begin{pmatrix} x_G \\ y_G \\ z_G \\ 1 \end{pmatrix} \quad (1.2)$$

Notation $T_{A \leftarrow B}$ means a transformation from the coordinate system B to the coordinate system A (the subscript should be read from the right to the left in the same order as matrices multiplication is performed). In the above equation p_I is some point in the US image space, where u and v are pixel coordinates, s_x and s_y are scaling coefficients translating pixels to millimetres, and p_G is the mentioned point in the global coordinate system. $T_{S \leftarrow P}$ is known from position sensor measurements. $T_{G \leftarrow S}$ usually depends on the location of position sensor's stationary part in relation to the imaged object. $T_{P \leftarrow I}$ is the unknown calibration matrix

1.2. Ultrasound calibration task

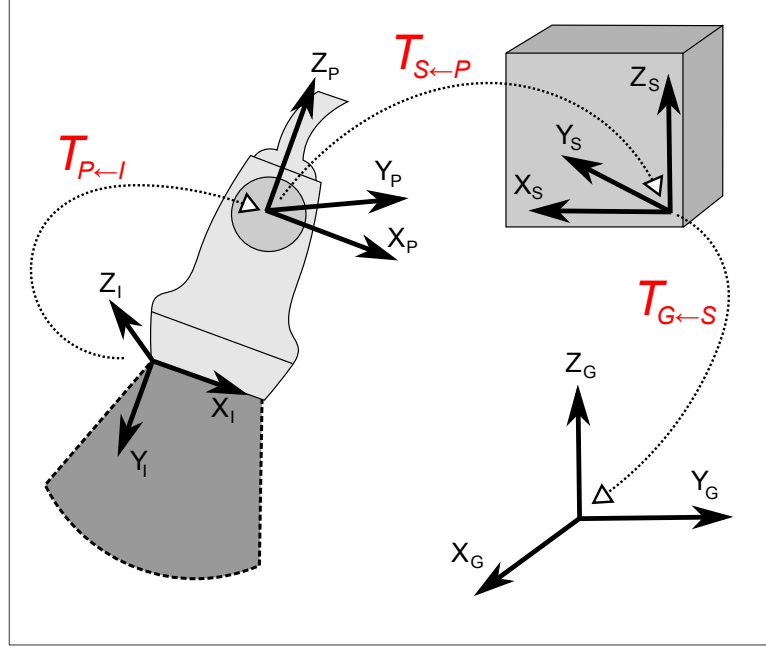


Figure 1.1: Calibration coordinate systems: US image (I), position sensor's mobile part (P), position sensor's stationary counterpart (S), global (G) coordinate systems.

that should be found from the provided equation. A rigid transformation in 3D has 6 degrees of freedom (DOF): 3 rotations (α, β, γ) and 3 translations (x, y, z). According to this notation calibration matrix can be found by minimization of an objective function that refers to the deviation between the expected position and the measured position of the corresponding landmarks. For the minimization one of the standard algorithms, e.g. least squares like in [61] or Levenberg-Marquardt like in [73]), may be taken. Equation (1.3) shows the objective function for N data measurements:

$$\min_{\alpha, \beta, \gamma, x, y, z} \sum_{i=1}^N (T_{G \leftarrow S} \cdot T_{S \leftarrow P} \cdot T_{P \leftarrow I}(\alpha, \beta, \gamma, x, y, z) \cdot p_I - p_G) \quad (1.3)$$

The rotation part of the transformation matrix can be represented in a variety of ways (quaternions, Euler angles in different order). As an example is the $x - y - z$ Euler rotation scheme [47]. Three rotations through γ, β and α angles are performed around x -axis, y -axis and z -axis accordingly starting from the x -axis rotation and ending with the z -axis rotation.

$$\begin{aligned}
 T_{A \leftarrow B}(\alpha, \beta, \gamma, x, y, z) &= \text{Translate}(x, y, z) \cdot \text{Rotation}_z(\alpha) \cdot \text{Rotation}_y(\beta) \cdot \text{Rotation}_x(\gamma) = \\
 & \begin{pmatrix} 1 & 0 & 0 & x \\ 0 & 1 & 0 & y \\ 0 & 0 & 1 & z \\ 0 & 0 & 0 & 1 \end{pmatrix} \begin{pmatrix} \cos \alpha & -\sin \alpha & 0 & 0 \\ \sin \alpha & \cos \alpha & 0 & 0 \\ 0 & 0 & 1 & 0 \\ 0 & 0 & 0 & 1 \end{pmatrix} \begin{pmatrix} \cos \beta & 0 & \sin \beta & 0 \\ 0 & 1 & 0 & 0 \\ -\sin \beta & 0 & \cos \beta & 0 \\ 0 & 0 & 0 & 1 \end{pmatrix} \begin{pmatrix} 1 & 0 & 0 & 0 \\ 0 & \cos \gamma & -\sin \gamma & 0 \\ 0 & \sin \gamma & \cos \gamma & 0 \\ 0 & 0 & 0 & 1 \end{pmatrix} = \\
 & \begin{pmatrix} \cos \alpha \cdot \cos \beta & \sin \alpha \cdot \sin \beta \cdot \sin \gamma - \cos \alpha \cdot \cos \gamma & \cos \alpha \cdot \sin \beta \cdot \cos \gamma + \sin \alpha \cdot \sin \gamma & x \\ \sin \alpha \cdot \cos \beta & \sin \alpha \cdot \sin \beta \cdot \sin \gamma + \cos \alpha \cdot \cos \gamma & \sin \alpha \cdot \sin \beta \cdot \cos \gamma - \cos \alpha \cdot \sin \gamma & y \\ -\sin \beta & \cos \beta \cdot \sin \gamma & \cos \beta \cdot \cos \gamma & z \\ 0 & 0 & 0 & 1 \end{pmatrix}
 \end{aligned}$$

To perform a calibration process it is common to use a device with known geometrical properties called ultrasound phantom [41, 61]. The main idea is to obtain US images that represent phantom features and then find a spatial relationship between the positions of these features on the ultrasound image and in the 3D phantom space.

1.3 Ultrasound calibration phantoms

Ultrasound phantoms may be classified according to the type of their landmarks – its features used for data acquisition and detection. There is a huge variety of US phantoms satisfying various calibration requirements providing different accuracy, speed of calibration, manual or automatic data acquisition and segmentation, and many others. There is no known solution outperforming all the others, the exact calibration phantom better suiting the concrete application must be selected individually according to system objectives.

1.3.1 Point phantoms

A point phantom consists of a single point or multiple points target which is imaged from a large set of positions and orientations. State et al. use a 4 mm bead [81]. Barratt et al. [7, 8] use a metal pinhead. Legget et al. [53] and Leotta et al. [55] take a 1.5 mm brass sphere suspended by a thread in a water tank. Pagoulatos et al. [67] use 2.5 mm plastic beads. Zhang et al. [89] use a tip of an electromagnetically tracked needle. Amin et al. use a 1 mm steel ball [4]. Lindseth et al. use a 2 mm spherical pin head [58].

Though a point phantom is a simple device, calibration with it can be a rather time-consuming process. Firstly, a large number of US images (more than the quantity of unknowns in the calibration equations) should be obtained, and each time the US probe should be accurately aligned with a small point object. Secondly, automatic segmentation of single points seems not to be reliable.

1.3. Ultrasound calibration phantoms

Almost all of the above mentioned groups report manual points segmentation. Both these peculiarities notably increase the calibration procedure time.

1.3.1.1 Cross-wire phantom

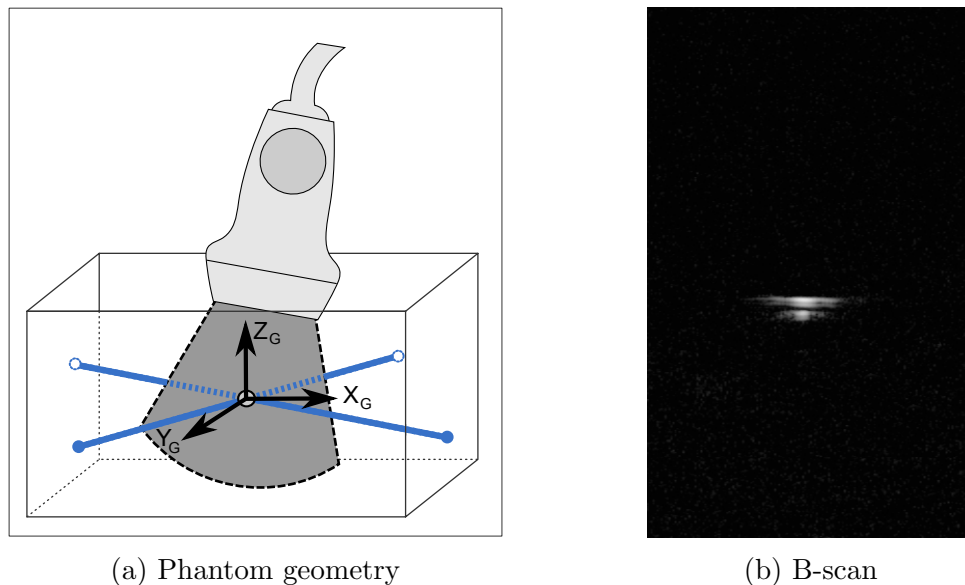


Figure 1.2: Cross-wire phantom.

A cross-wire phantom is a commonly used calibration device (Detmer et al. [27], Barry et al. [9], Trobaugh et al. [83], Mears et al. [60], Anagnostoudis et al. [5], Huang et al. [43], Krupa [50]), mostly because of its construction easiness. It can be arranged to the point phantom class because both these methods are based on mapping of a point target from one space to another. However, the cross-wire phantom's geometry is different from the point phantom. The phantom is composed of two intersecting wires (nylon like in [83], cotton [27, 43], etc.) that are placed into a water tank. There are also approaches with more than one intersection point (diagonal-phantom from Lindseth et al. [57, 58]), however the calibration procedure remains the same as for the single intersection. The intersection point is imaged by an ultrasound probe from different positions and orientations. This landmark produces a small cross (or a part of a cross) on an US image. The centre of the cross should be detected and then matched to the correspondent reference coordinates in the phantom coordinate system. For the purpose of convenience and calculations simplifying the centre of phantom's coordinate system is placed into the wires' intersection, which transforms the

equations (1.1) and (1.2) into the (1.4) [73]:

$$\begin{pmatrix} 0 \\ 0 \\ 0 \\ 1 \end{pmatrix} = T_{W \leftarrow S} \cdot T_{S \leftarrow R} \cdot T_{R \leftarrow B} \cdot \begin{pmatrix} s_x \cdot u \\ s_y \cdot v \\ 0 \\ 1 \end{pmatrix} \quad (1.4)$$

This equation contains 12 unknowns: 6 (3 rotations + 3 translations) for the calibration matrix $T_{R \leftarrow B}$ and 6 for the $T_{W \leftarrow S}$ matrix. However, if we look at matrix $T_{W \leftarrow S}$ it is obvious that its orientation can be ignored, because the matrix satisfies the equation (1.4) at any orientation. This means that 3 rotations of the $T_{W \leftarrow S}$ are unidentifiable parameters and can be ignored (e.g. set to 0). This ends up with 9 unknowns for the system (here it is assumed that scaling coefficients s_x and s_y are known from the US system settings; if not, two additional scaling parameters can be treated as unknowns).

This method's accuracy strongly depends on the cross centre detection quality, which is usually done manually. Both this and the manual transducer-cross alignment task are rather time-consuming operations.

1.3.1.2 Spherical landmarks

Comparing to points, spheres suit better for semi-automatic or automatic calibration methods. A sphere has more features that can be extracted from observed images. When a spherical object is imaged using the B-mode it appears on the US image as a circle or an arc that may be automatically segmented. The sphere's centre is treated as a landmark point and may be detected from the sphere's central section.

Certainly, the circle's representation on the US image strongly depends on the object's material. Different research groups test various materials for this purpose. Brendel et al. [18], Atkinson et al. [6], Gooding et al. [37] use a liquid filled table tennis ball. Treece et al. [82] use a grid of 2 mm nonechogenic spheres, Wang et al. [86] use 5 mm ceramic balls. Sauer et al. in [79] and Khamene et al. in [49] use the same balls that are a part of an optical tracking system.

There is a variety of available automatic methods for circle detection on the images, e.g. the Hough transform [39]. Sauer et al. [79] use manual detection based on the template fitting, but the authors mention, that the process can be easily automated. Brendel et al. apply a semi-automated processing on a huge amount of balls images taken from different position to determine the radius and centre of the ball [18]. Treece et al. [82] use a nonlinear optimization algorithm to align the acquired US data with known phantom geometry, as well as Wang et al. [86].

1.3. Ultrasound calibration phantoms

The main problem in obtaining the sphere's central point on a 2D US image is to align the probe with the sphere in the way, that the ultrasound beam goes right through the sphere's centre. Gooding et al. place a cross-wire phantom into the ball to solve this task [37], in other applications it has been performed manually.

1.3.1.3 Stylus

A stylus is a 3D spatial positioning device (also called a 3D localizer or a pointer) which can be used for the US calibration instead of a calibration phantom (Muratore and Galloway [64], Poon and Rohling [71], Hsu et al. [42]). A stylus usually consists of a set of tracked markers and a sharpened tip (see Fig. 1.3). When the tip is pointed towards any spatial point its coordinates can be obtained from the position detector that tracks the markers which uses the known tip-to-detector rigid body transformation. This transformation is either known from the manufacturer or can be calculated during the pointer calibration.



Figure 1.3: Stylus for passive optical tracking from *Northern Digital Inc.*

The US calibration using a stylus is similar to the calibration with a point phantom since a point target is measured. During the data acquisition the tip of the stylus is imaged with the US probe while pointer's tracked part is moved around (usually rotated) to provide sufficient calibration data from different orientations. Using the position detector's readings each point's coordinates are obtained in the global space. Coordinates in the image space are received from an US image. This step suffers from the main point calibration drawback: point segmentation is normally done manually or semi-automatic since point echoes are not well-formed on an US image. Finally, the calibration transformation is obtained from the equation (1.1).

However, there are some disadvantages in such method. The main one is the necessity to scan a tiny point object that, according to the beam width property, is visible on the US image even if the probe is not accurately aligned with the tip. This leads to a disposition error up to several millimetres [42]. The other disadvantage is that the calibration procedure requires considerable amount of time and an experienced user.

1.3.2 Wire phantoms

1.3.2.1 Three-wire phantom

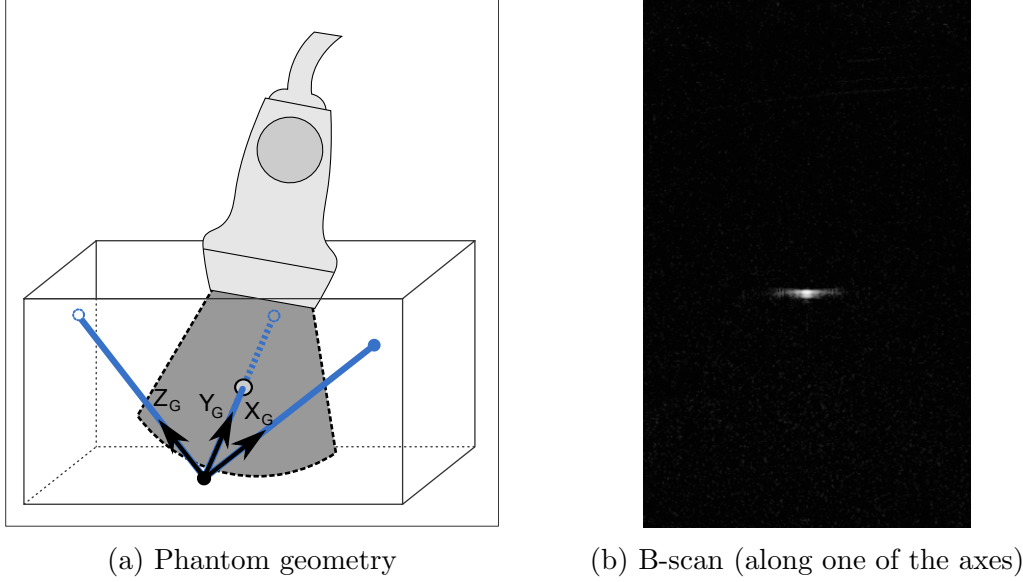


Figure 1.4: Three-wire phantom.

A three-wire phantom is constructed using three mutually orthogonal wires that are placed into a water tank similarly to the cross-wire phantom [19, 73, 41]. However, the scanned object is not the wires intersection point, but each wire itself. The wires coincide with the axes of the phantom coordinate system whose origin is defined in the wires intersection point. Each wire is scanned separately along its axis from different probe positions that gives a single dot on the US image. The equation for each of these dots looks as follows:

$$T_{W \leftarrow S} \cdot T_{S \leftarrow R} \cdot T_{R \leftarrow B} \cdot \begin{pmatrix} s_x \cdot u \\ s_y \cdot v \\ 0 \\ 1 \end{pmatrix} = \begin{cases} \begin{pmatrix} x & 0 & 0 & 1 \end{pmatrix}^T & \text{for } x\text{-axis} \\ \begin{pmatrix} 0 & y & 0 & 1 \end{pmatrix}^T & \text{for } y\text{-axis} \\ \begin{pmatrix} 0 & 0 & z & 1 \end{pmatrix}^T & \text{for } z\text{-axis} \end{cases} \quad (1.5)$$

This equation contains 12 unknowns: 6 for the calibration matrix $T_{R \leftarrow B}$ and 6 for the $T_{W \leftarrow S}$ matrix.

Due to the fact that no accurate probe alignment with the wires is required, the data acquisition procedure becomes less time-consuming. However, the detection of landmarks on the acquired US images remains a challenging task, manual

1.3. Ultrasound calibration phantoms

segmentation is usually required. Calibration accuracy depends also on the quality of the phantom assembly. The wires should be straight and orthogonal that it not very easy to achieve in practice.

1.3.2.2 Z-phantom

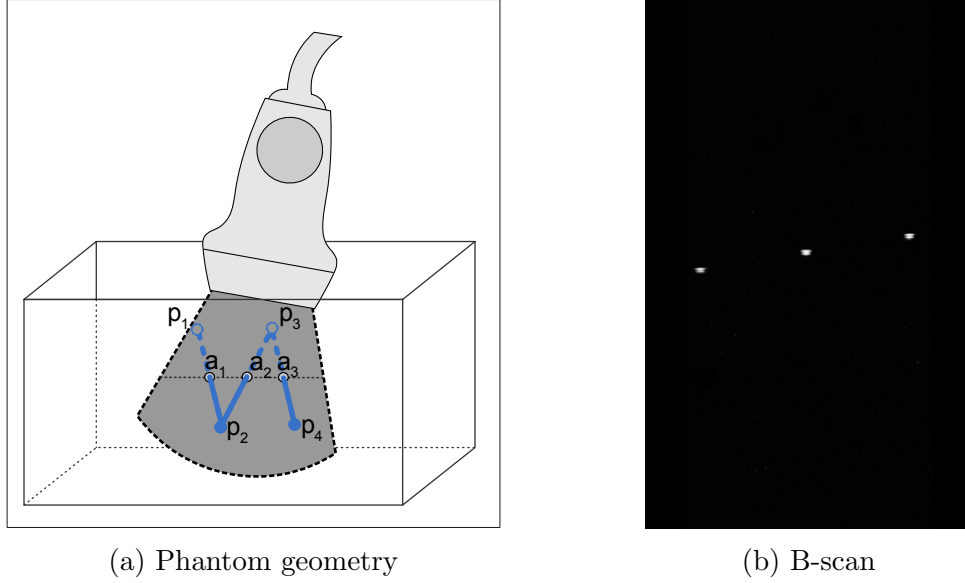


Figure 1.5: Z-phantom.

Another simplification of the calibration procedure is provided using a so called Z-phantom. The phantom consists of wires located in a Z shape [23, 36, 40] (or N shape in other works [68, 90]) as shown on Figure 1.5. The wires are mounted in a water bath where their location in the phantom coordinate system is known (for example by measuring the wires' ends using a spacial localizer).

Let us denote the i -th segment of the Z -shape as $p_i p_{i+1}$. The image plane intersects the wires $p_1 p_2$, $p_2 p_3$ and $p_3 p_4$ at the points a_1 , a_2 and a_3 (calibration target landmarks). Since the wires $p_1 p_2$ and $p_3 p_4$ are parallel, we have the similarity of the triangles $\triangle a_1 p_2 a_2$ and $\triangle a_3 p_3 a_2$. As far as the distances $a_1 a_2$ and $a_1 a_3$ can be measured from the B-scan, we can get the coordinates of the point a_2 in the phantom coordinate system:

$$a_2^W = p_2^W + \frac{|a_2^B \ a_1^B|}{|a_3^B \ a_1^B|} \cdot (p_3^W - p_2^W)$$

$$\begin{pmatrix} a_{2x}^W \\ a_{2y}^W \\ a_{2z}^W \\ 1 \end{pmatrix} = T_{W \leftarrow S} \cdot T_{S \leftarrow R} \cdot T_{R \leftarrow B} \cdot \begin{pmatrix} s_x \cdot a_{2x}^B \\ s_y \cdot a_{2y}^B \\ 0 \\ 1 \end{pmatrix} \quad (1.6)$$

Z-phantom in different variations is used by Cameau et al. [23, 24] (thin plastic tubes filled with liquid), Gobbi et al [36] (one Z-bar), Pagoulatos et al. [68] (30 N-shape nylon string fiducials in 5 planes), Lindseth et al. [58] (pyramid-phantom), Boctor et al. [15] (N-form), Zhang et al. [90] (several N-shape fiducials), Chen et al. [20, 21] (double-N phantom), Hsu et al. [40] (Z-phantom with a rubber membrane on top). Some of the research groups report fully automatic calibration procedures (Chen et al. [21], Hsu et al. [40]).

1.3.2.3 Other wire phantoms

The idea of scanning a wire to receive a dot echo is also applied in some other phantoms.

Boctor et al. [16] propose the Hopkins phantom from two parallel plastic plates with parallel nylon wires stretched between them. The phantom is used in combination with the multi-sided transparent water tank for phantom immersion. The wires layout provides more detectable features per US image and therefore requires less images for the accurate calibration than the cross-wire or the three-wire phantom. The authors use a semi-automatic method for landmarks detection.

Liu et al. [59] built a plexiglass cube with a triangular pyramid from silk threads mounted inside. These wires are stretched between two opposite walls of the cube. The scanning procedure is designed to intersect these three wires forming a triangular cross section as a target. This phantom is proposed to reduce the influence of the ultrasound beam thickness effect.

Beasley et al. [11] constructe their phantom from two parallel metal plates with string wires running between them as a "ladder". Such a construction produces a set of points on one B-scan, namely 14 points for a 12 cm probe depth.

Poon and Rohling [71] use an IXI-form wire phantom which is very similar to the N-phantom but an extra wire adds additional features.

1.3.3 Plane phantoms

Plane (wall) phantoms are based on the idea that a plane imaged by an US probe appears on the correspondent B-scan as a straight line. The plane phantom provides more rapid calibration than the wire phantom [61] since it is much easier to correctly detect a line than a dot on the US image. Line detection can be performed automatically.

1.3. Ultrasound calibration phantoms

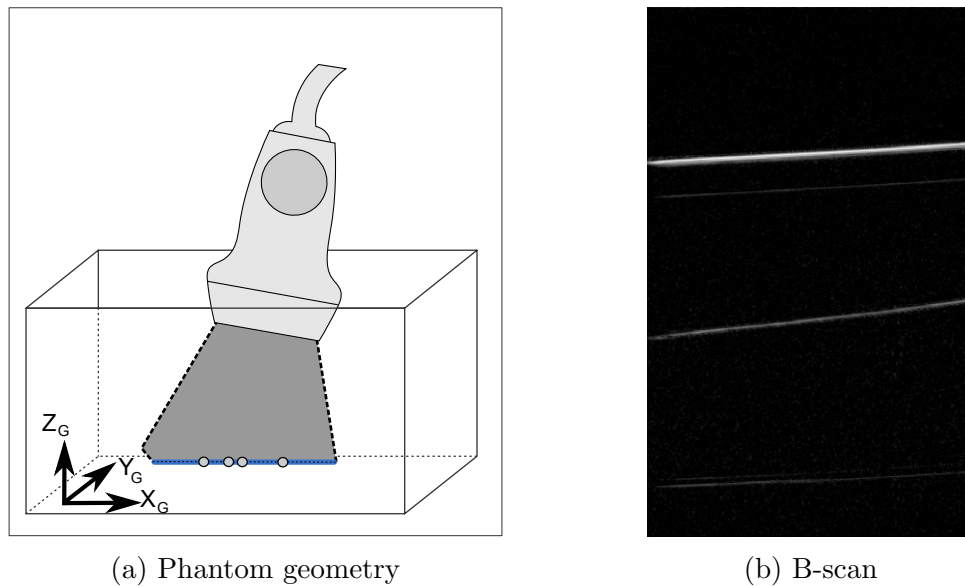


Figure 1.6: Single-wall phantom.

1.3.3.1 Single-wall phantom

A single-wall phantom (presented by Prager et al. [73]) is a simple water bath where the bath's bottom itself is imaged. Some variations are proposed by Rousseau et al. [74] (a plexiglass plate in a water bath), Poon and Rohling [71] (a cube), Baumann et al. [10] and Langø [51] (a nylon mesh membrane), Najafi et al. [65] (aluminium plate). Dandekar et al. [25] simulate a plane by using two coplanar wires strung parallel to the water tank's bottom.

Data acquisition is performed by scanning a plane from different orientations from that a strong line appears on the B-scan. Each line is then automatically detected. Any point on this line can be treated as the calibration target landmark. For this purpose it is assumed that the phantom coordinate system is aligned with the imaged plane, which corresponds to the XY -coordinate plane.

Comparing to the point and wire phantoms the single-wall phantom has some advantages. Firstly, there is no need to assemble a special device since a water bath itself can be used for the calibration. Secondly, the calibration can be performed more rapidly because automated echo detection can be done. However, there is a drawback called a beam-width problem (see Fig. 1.7) caused by the US beam nature. When imaging from oblique angles an echo from the point A is received earlier than an echo from the point B (see Fig. 1.7). This causes the incorrect line positioning on a B-scan. In addition, the line loses sharpness and intensity because the reflection away from the probe increases.

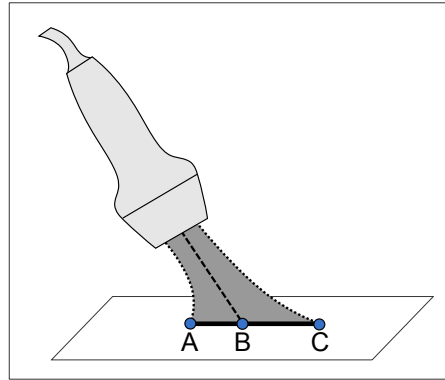


Figure 1.7: Beam width problem.

1.3.3.2 Cambridge phantom

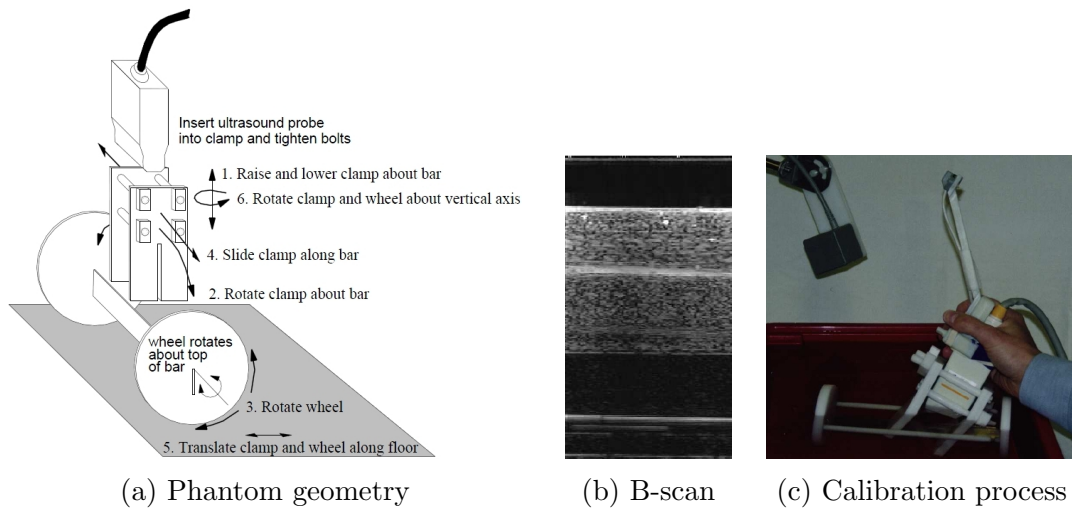


Figure 1.8: Cambridge phantom (Prager et al. [73]).

The Cambridge phantom is a special plane phantom that is designed to overcome the beam width problem (Prager et al. [72]). The phantom is made of a clamp mounted around the US probe and a thin bar with wheels connected to the clamp. The bar serves as an imaged plane instead of the water bath's bottom and is constructed to stay in the centre of the beam while the probe is moved in various directions. After attaching the clamp to the probe the user should adjust the probe – to align it with the bar (which may be somewhat complicated according to [41]). Then the bar should be scanned from different positions which gives a strong, automatically detectable edge. The following calibration procedure steps remain the same as for the single-wall phantom.

The Cambridge phantom based calibration is also implemented by Ali et al.

1.3. Ultrasound calibration phantoms

[3] and Varandas et al. [84].

1.3.3.3 Plane phantom with wires

Dubouski et al. [28] introduce a hybrid plane phantom with wires that combines the properties of both plane and cross-wire phantoms (see Fig. 1.9). This approach simplifies the landmarks detection and increases the calibration accuracy. Authors also suggest an automatic landmarks detection algorithm. The phantom consists of a plexiglass plate with two wire crosses on its top surface. Each cross acts like a cross-wire phantom. One of them can be used as the main landmark, the other is used either as a control landmark or as additional calibration marker. The calibration procedure remains the same as for the cross-wire apart from one fact: the plane gives a straight line on the acquired image at that the landmark point is located (see Fig. 1.9). It provides additional information to detect the landmark.

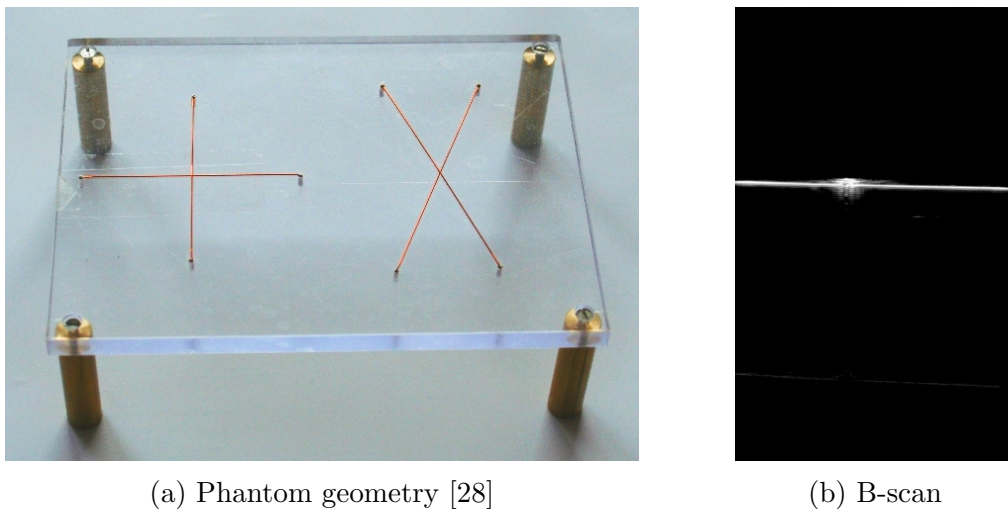


Figure 1.9: Hybrid plane-wire phantom.

1.3.4 Alignment phantoms

Alignment in the ultrasound calibration procedure means positioning the US probe accurately in such a way that it captures some exact part of the imaged object. From this point of view all point phantoms belong to this class because a user needs to carefully align the transducer with the small object representing a target point landmark. The difference is that the alignment phantom is usually an object with more than one landmark or a landmark different from a point. In contrary to the point phantom the alignment phantom typically has a 2D shape,

which leaves less alignment DOF since it requires capturing from some certain, not arbitrary positions.

1.3.4.1 Shaped board

Sato et al. [78] use a special shaped thin board with 3 vertices. The US probe should be aligned with all three vertices at a time (see Fig. 1.10). Reference spacial locations of the vertices are determined using a position localizer.

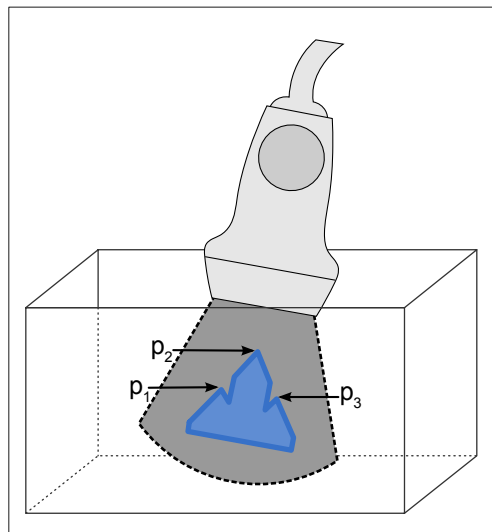


Figure 1.10: Sato et al. shaped board alignment phantom.

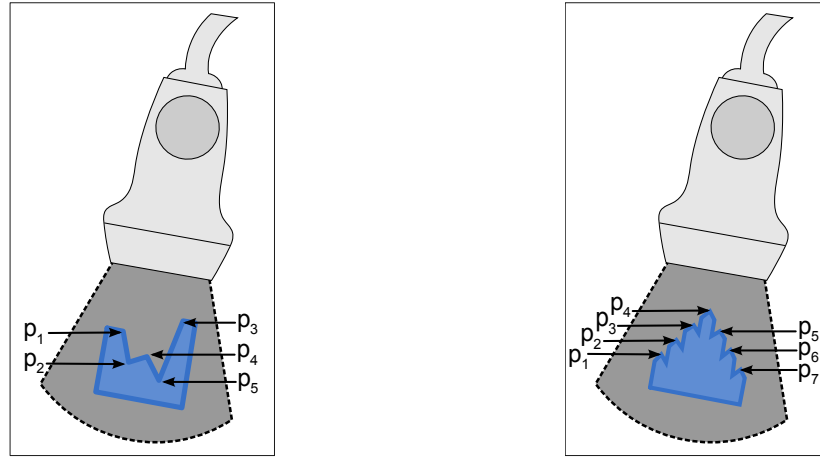
Berg et al. [12] use a jigged membrane with five corners immersed into a water bath, where the probe should be aligned with the membrane plane (see Fig. 1.11a). Corners location in the phantom space are measured with the position sensor.

Welch et al. [87] use an approach similar to Sato et al. [78]. The phantom consists of a thin acrylic plate with seven edges (see Fig. 1.11b).

1.3.4.2 Mechanical instrument

Gee et al. [33] introduce a 2D-alignment phantom called the Mechanical instrument, which requires only a single B-scan to proceed the calibration and no manual alignment from a user. The imaged object of the phantom is a frame with wires strung on it and the wedges attached to these wires (see Fig. 1.12). The frame is placed into the device body which has a gantry holding the transducers, a position sensor, and adjustment controllers. Due to the precise construction all transformations between device parts are known, including the rigid body transformation between the gantry and the position sensor. During data acquisition

1.3. Ultrasound calibration phantoms



(a) Berg et al. jagged membrane

(b) Welch et al. alignment phantom

Figure 1.11: Other shaped board alignment phantoms.

the US probe should be aligned with the frame plane by adjusting the micrometers that control the probe position. The micrometers readings are then used to receive the transformation between the wires and the gantry. Plane alignment is done by controlling the echo from the wedges, which should give an exact symmetric reflection when being aligned. The beam is aligned with three pair of wedges at a time, which are mounted on a wire in the opposite directions to each other. A properly aligned beam passes through the wedges pair in the middle. In this case both wedges' diagonal faces give symmetrical image, otherwise the reflection from one wire is higher than from another. This design helps to overcome the beam width problem. The wedges' echoes are then detected by a semi-automatic segmentation algorithm.

The calibration can be performed using a single US image and does not require much user experience. The experiments demonstrate high accuracy and precision of the method. However, the main disadvantage is the complexity of the phantom itself, which is neither simple nor easy to construct.

1.3.4.3 Planar strings array

Leotta [54] introduce a phantom that consists of coplanar wires arranged in a plane with small beads on them and a set of additional strings used for orientation guidance (see Fig. 1.13). One bead placed on the top string serves as a reference point, it's location is fixed and measured relative to the phantom coordinate system in advance. Other beads are placed on arbitrary positions on other strings and serve as visual markers. During data acquisition the US probe is aligned with the strings plane and the reference bead is visualized. Strings plane position is obtained by measuring three wires' ends with a stylus after the phantom has

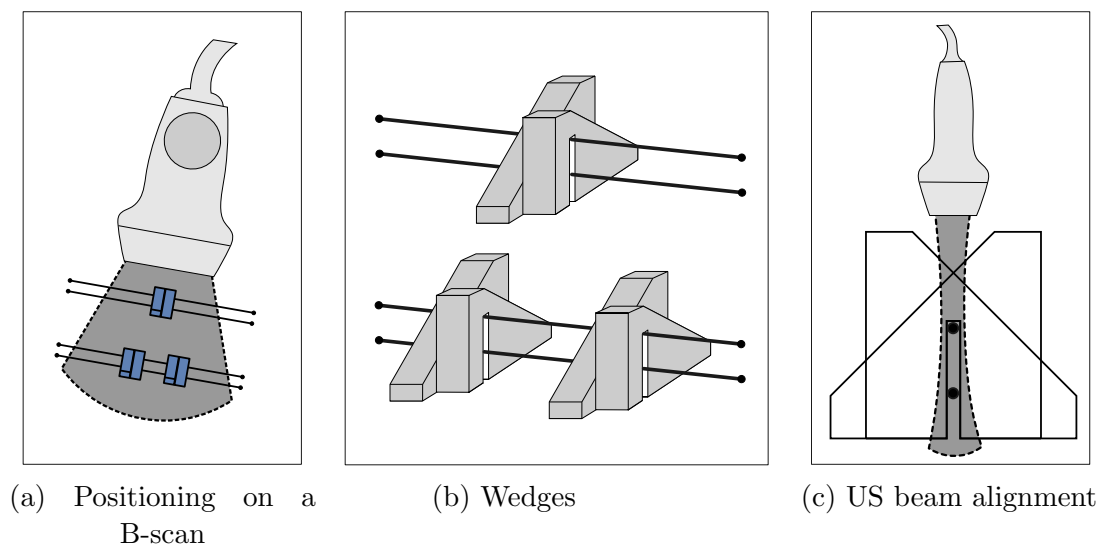


Figure 1.12: Gee et al. mechanical instrument.

been immersed into the water. Manual point segmentation is required to detect the position of the reference point on the B-scan. The authors report that the calibration procedure takes from 10 to 15 minutes, however the calibration quality strongly depends on the ability of the user to precisely align the US probe.

1.3.4.4 Wedges phantom

In this section we talk about the calibration task and its solutions for a single transducer. Similar mathematical principles can be applied to the task of dual transducers alignment and calibration. The goal of such dual system is to compose the data from both transducers into one resulting dataset. This task is crucial for example in spacial compounding used for speckle reduction. In this case the calibration should provide the transformation from one transducer to another.

Abeysekera and Prager [2] present their wedge phantom visible from both transducers for this task. The phantom design is inspired by the work of Gee et al. [33] who used wedges (see Fig. 1.12) in their mechanical instrument. The phantom consists of two identical parts located orthogonally to each other. Each part is made of two wedges pairs of different size. Cross-over points of each pair intersect in the same plane. Data acquisition step consists in aligning each probe with the correspondent wedges to receive the cross-over plane image. The calibration transformation is obtained by matching the wedge model to the patterns extracted from the B-scan applying the optimization algorithm.

The authors report 1.6 mm mean accuracy error calculated by mapping points from one transducer to another. The calibration carried out with the N-fiducial

1.3. Ultrasound calibration phantoms

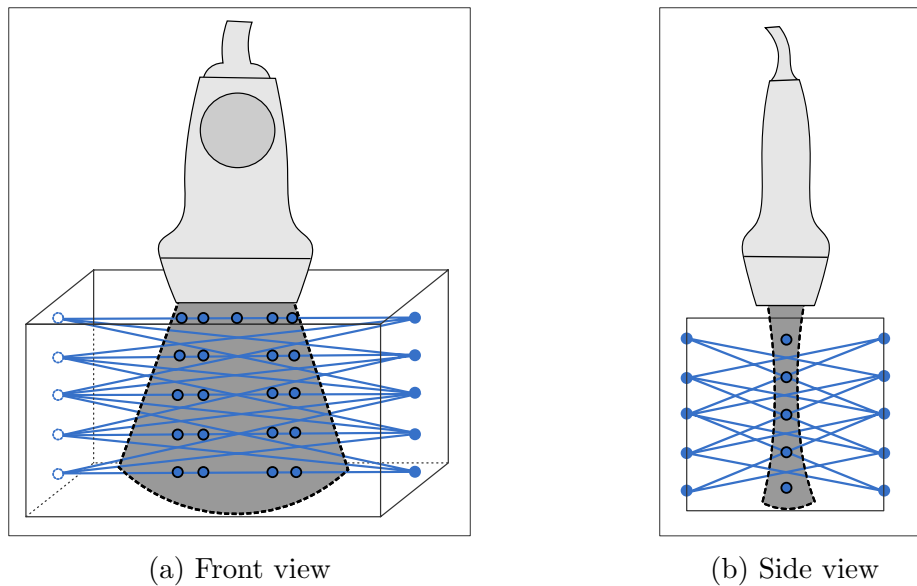


Figure 1.13: Leotta alignment phantom.

phantom shows similar results to the wedge phantom.

1.3.5 Registration phantoms

Using registration technique for calibration is a principally different approach comparing to the described above. It is based on the idea of matching the US data of the phantom to it's model obtained from another imaging modality like CT or magnetic resonance imaging (MRI). The main advantage of such calibration technique is the independence of the method from the phantom form. Phantom shape should only provide US images distinguishable from different positions and orientation. Non-symmetrical phantoms usually satisfy this requirement.

Blackall et al. [13] introduce their calibration method based on registration of a gelatin phantom. The calibration algorithm finds parameters that provide the best registration between the US images and 3D data in phantom's space by minimizing the similarity measure between these two datasets. Selection of an appropriate similarity measure is an important task, since registered datasets are from different domains that should be somehow matched to each other. Blackall et al. use the normalized mutual information (NMI) measure which is proved to align images from different image modalities accurately:

$$I(W, B) = \frac{H(W) + H(B)}{H(W, B)} \quad (1.7)$$

Here $H(\cdot)$ is the marginal entropy of the image, $H(W, B)$ is the joint entropy

of both images, both entropies are calculated from the joint histograms. For each US image the correspondent location of every image pixel in the phantom space is calculated (using equation (1.1)). The intensity of the point in the model is interpolated using its eight voxel neighbours and is contributed to the joint histogram together with the intensity of the source US image pixel. The calibration transformation T_B is then found as a transformation maximizing the similarity measurement I as a function T of the phantom model points W and the US data points B :

$$T_B = \arg \max_T I(W, T(B)) \quad (1.8)$$

The phantom is constructed from a gelatin block placed into a rigid container. To enhance the shape's irregularity some molten gelatin is added onto the base and formed into asymmetric structures of different depths and orientations. The phantom model is built using MRI. The authors report a calibration error comparable to the point-based technique that is rather high. The proposed method takes about 2 minutes for data acquisition and registration and is carried out fully automatically.

Peterhans et al. [69] perform the US-CT calibration in their joint calibration and registration framework. The optimization is done using the Levenberg-Marquardt algorithm with the RMS distance error as a cost function. In this approach femur and vertebra bones are taken as phantoms.

As well as for 2D calibration, the registration method is used by some groups for the 3D US probe calibration.

Lange and Eulenstein [52] take the commercially available device from Computerized Imaging Reference Systems as a phantom and implement the US to CT registration. Points distance RMS is used as a similarity measure.

Huang et al. [44] use a polyvinyl alcohol cryogel object of an arbitrary shape with sufficient number of detectable features (no special phantom geometry is required). Registration is done by maximizing the normalized cross correlation metric. For calibration evaluation and validation a hydrogel heart phantom with fiducial markers is used.

Chapter 2

Ultrasound Fracture Analysis Scanning System

2.1 Automated ultrasound systems

In this work we present a novel calibration solution for the UFASS – an automated scanner for human extremities, which replaces the computer tomography diagnostics in several cases. Automatic scanning procedure opens the possibility of fast and precise diagnostics where a 3D model of a scanned object can be build and analysed. This would be not possible in the case of freehand ultrasound system. Freehand ultrasound transducers have their advantages and scope of application. However, there are some reasons to construct an automated ultrasound scanner rather than to use a freehand one, namely:

- Freehand ultrasound investigation is a time consuming process which requires persistent expert's attention. In case of considerable amount of patients in the clinical practice it is desired to shorten the duration of a single investigation and increase it's simplicity.
- Ultrasound modality often gives diverse results that can be treated differently. Is is liable to different types of artefacts which is a source of confusion for the interpreter [30]. Obtained images may often depend on tiny probe movements. In these conditions it is important to standardize the scanning procedure and to be able to obtain comparable data.
- Investigation conclusion depends fully on the expert's opinion. Different experts may base the decision on their unique experience, have bias, be less competent than the others. It would be advisable to make the diagnostics independent from a human factor.

An automated ultrasound scanner is ought to solve the listed tasks. The idea of operating an ultrasound probe with an automated motion controller is used in

Chapter 2. Ultrasound Fracture Analysis Scanning System

medical systems as well as in industrial applications. Present solutions vary from a robot arm attached to a transducer that models expert's movements to more complex robotised devices like breast cancer diagnostics system or ultrasound tomography. Between the known automated ultrasound scanners there are:

- An automatic ultrasonic inspection device for high-speed and accurate quality determination of spot welded parts [88]. Another patent [48] describes the spot welds automatic testing method.
- A general system for medical ultrasound with a robot arm under the shared control of an operator and computer [76].
- A method for low-level radiation puncture or biopsy in a combined C-arm x-ray and ultrasound system [17].
- Carotid artery examination method with a robot-controlled ultrasound transducer motion [91, 77].
- Abdominal screening ultrasound imaging system for telemedicine invented in Japan [1].
- *OTELO* ultrasonic system for patients remote investigation developed in France and Italy [66, 32, 26]. The system is equipped with the robot-controlled ultrasound probe holder that reproduces the hand movements of an expert (see Fig. 2.1).



Figure 2.1: *OTELO* tele-echography system [66].

- *TER* – the telesonographic system with an ultrasound transducer remotely rotated and tilted inside a fixed frame [85].
- *HIPPOCRATE* – project presenting the kinematic design with a 6-DOF transducer [70].
- *GABIE* project with its transducer attached to a surgical tool for endoscopic telesonography [31].
- *Acuson S2000 Automated Breast Volume Scanner (ABVS)* from Siemens introduced for women mammography in 2008. According to the report automated scanner reduces the investigation time from 30 to less than 15 minutes in comparison to the standard manual technique [75].
- *Ultrasound tomography* scanner [34, 38, 80, 46]. The system is a cylinder

2.2. UFASS

with many transducers attached on the periphery. Despite the fact that currently the device is too slow for clinical application the idea is hoped to be used for early breast cancer detection. In Karmanos Cancer Institute [29, 35, 56] a similar approach is used.

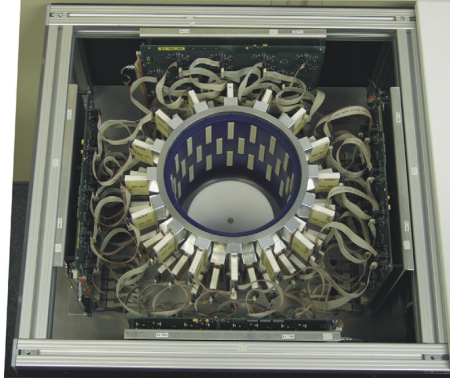


Figure 2.2: An ultrasound tomography system [34].

What all these systems have in common is a some kind of transducers positioning mechanism that operates the probe motion according to some program and provides transducer's coordinates in space. Some systems may provide up to 6 DOF [70], others include only several rotation and translation navigation possibilities. In contrary to the freehand ultrasound there is no human intervention while operating the transducer that means the scanning procedure is repeatable and non-random.

2.2 UFASS

2.2.1 Design and application

UFASS (Ultrasound Fracture Analysis Scanning System) is constructed as an automatic ultrasound scanner for orthopaedics which makes use of the benefits of automated ultrasound systems over freehand ones that are described above. This is an alternative to the CT modality for precise analysis and reconstruction of extremities injures, such as bones fractures and deformities. The scanner is planned to provide diagnostic information, e.g. bone surface reconstruction and 2D/3D visualisation [14]. The main benefits of the system comparing with the CT investigation are:

- Absence of radiological load;
- Non-invasiveness and contactlessness;
- Low costs;

- Compact size and easiness in implementation.

The UFASS does not fully replace CT for extremities study. Since ultrasound modality provides not perfectly clear images with noisy objects contours it is possible that some unclear clinical cases will require additional CT investigation. However, the UFASS is expected to cover the majority of cases which is a significant advance, especially for children and pregnant women, for whom CT investigations are not recommended.

The UFASS scanner consists of a body and a host PC. The host PC has the beam forming controllers, US data acquisition, processing, and displaying software. The body is made of an inner removable tank (which is filled with water), two ultrasound transducers, and the transducers motion controller. Through the fine precision mechanism of the controller both transducers can be rotated around a fixed axis over 360 degrees and moved in the vertical direction (see Fig. 2.3a). Transducers' beam emission is directed toward the scanner rotation centre. The system is also equipped with the pluggable hand (see Fig. 2.3b) and leg holders which can be placed into the scanner body to fixate an extremity.

Patient examination is intended to take a couple of minutes and is proceeded in the following way:

1. Preparation step. A fresh clean water tank is taken, attached to the scanner and filled with water.
2. Calibration step. System recalibration is performed and a new calibration matrix obtained.
3. Data acquisition step. An extremity is placed into the middle of the water tank and fixated with the appropriate holder. During this step the system's body is rotated and vertically moved around the extremity to obtain it's US scans from different positions and orientations. The extremity is released after this step is finished.
4. Data processing step. Bones detection is made on each single B-scan automatically and a 3D model of bones surface is reconstructed from all B-scans.
5. Finishing step. The water tank is removed and send to disinfection.

2.2.2 Prototype

At the moment of this research the UFASS production has not yet started and only the system prototype has been available (see Fig. 2.4). Comparing to the final clinical device the prototype has some construction differences, namely:

- The device body is not separated into a removable inner tank and an outer mechanical part with the transducers and motion controller. Both are combined in one cubic form container. This implies the transducers to be placed

2.2. UFASS



(a) Device architecture.

(b) Inner part with a hand holder.

Figure 2.3: UFASS model (©UltraOsteon GmbH).

inside the body, not outside.

- Half-automatic rotation and translation mechanism. The prototype is motor-free and rotation and translation are controlled by the fine mechanical screws. The motion curve and the steps are defined by these screws the same way as they would be defined by the controller, but the signal to move the transducer is given not automatically, but send manually by a user.

The differences listed above do not affect the scanner operation, they have an influence only onto the scanning procedure (more manual operations are required) and are made for the manufacturing simplicity.



Figure 2.4: UFASS prototype.

2.3 UFASS calibration requirements

The whole investigation with the UFASS would be not possible without the system calibration which is the process of obtaining the spatial transformation from the transducers' scan plane to their holder which is attached to the motion controller. The controller operates holder motion. The position of the holder relatively to the scanner is rigidly known from construction, but the relation between the transducer and the holder is unknown and varies a bit after attaching/reattaching the transducer at each investigation. The system uses 2D ultrasound transducers providing two-dimensional images which should be transformed into a 3D model. This requires a correspondent transformation from the 2D space to the 3D, and the calibration transformation is the first part of it. It can be obtained using the calibration procedure with the so called calibration phantom. The accuracy of this transformation directly influences the quality of the result 3D model. Even a small error may imply a huge displacement of the data in 3D space which would make the precise diagnostics impossible and the results unreliable.

The calibration procedure for the UFASS should be executed very often since the system is constructed in a way that for every investigation the inner part with a water tank is reattached from the mechanical part for sterilisation and replaced with a new one for every patient. This requires mechanical removal of the transducers that may lead to their displacement regarding the holding clamp. Since even the slightest displacement may disastrously increase the calibration error the calibration procedure should be performed when the transducers are attached back. This imposes the following requirements to the calibration procedure for the UFASS:

- **Robustness.**
Since the phantom and other system parts used for calibration would be often in use they should be robust and stable, containing no fragile parts which may deform after some time.
- **Low costs and construction simplicity.**
Since each clinical device must have its own calibration phantom the costs for it must be not too high in order not to increase the cost of the UFASS noticeably.
- **Execution simplicity and speed.**
Since the calibration may be required as often as each patient investigation is performed, it would directly increase the investigation time. This leads to the requirement that every calibration routine should be executed as quick and easy as possible in order not to increase the investigation duration and costs.
- **Self-sufficiency and expert-independence.**

2.3. UFASS calibration requirements

Since the calibration routine must be executed on place it would be most probably performed by clinical personnel. This means it should be that simple that an inexperienced user can perform it with no extra calibration specialists and devices involved. It also should not require from a user any complicated manual operations that would influence the calibration quality when being improperly fulfilled.

- **Distances range support.**

The scanner is constructed in a way that measurements may be done from several different distances from the transducer to the scanned object. It should be taken into account that both arms and legs should be scanned, and that the extremities may have different diameter depending on the patient's age and body constitution. It consequently requires to calibrate the device on setups with various distances from the transducer to the calibration phantom.

- **Positions and orientations variety support.**

The UFASS is equipped with two transducers oriented 90 degrees to each other in the vertical direction. The investigation procedure is designed in a way that a 360 degree scan must be obtained in the horizontal orientation. It requires a correspondent calibration which must support the phantom's visibility from all possible scanning positions.

- **Automatic image processing.**

Automatic landmarks recognition is the main requirement to the UFASS calibration procedure. It becomes absolutely essential when taking into account that the calibration procedure would be performed oft and must be easy, fast and precise. Phantom's landmarks detection is one of the most crucial part of the calibration procedure which influences the result significantly. Firstly, the procedure should not produce ambiguous image data. Secondly, an automatic features detection algorithm should be provided, since manual detection is usually the most time-consuming and error-prone part of the calibration task.

Naturally the calibration accuracy is also a very important factor. It is not mentioned in the list here because it is anyway clear that accuracy must be "the more the better". This criterion should be analysed if there are several possible calibration solutions that satisfy the formulated objectives. The accuracy of the most calibration phantoms starts from 0.3-0.4 mm RMS and ends over 1-1.5 mm. Most of the phantoms lie over the 0.5 mm RMS border, that value should be appropriate for our application as well.

2.4 Analysis of existing calibration techniques in application to UFASS calibration

In the first chapter the main calibration phantoms are presented. The basic classification of the phantoms is based on the type of the landmark that is detected during the calibration procedure and can be shortly described as following:

- **Point phantoms** (beads, cross-wire, spherical landmarks, stylus).
The landmark is a point-like object, either a real point like a small bead, or a part of some bigger object, e.g. the spheres centre or a stylus top. Gives a single dot on the US image.
- **Wire phantom** (three-wire, z-phantom).
The landmark is a point on a wire or several wires that are assembled into a configuration with several geometrical requirements. The wire is scanned in the orthogonal direction, each point of it is classified as a landmark. Each scan obtained this way gives a single dot on the US image.
- **Plane phantom** (single wall, Cambridge).
The landmark is a point on a plane, e.g. a plain surface of some object. A scan of a plane gives a line on the US image each point of that is classified as a landmark.
- **Alignment phantom** (shaped board, the mechanical instrument, wedges).
The landmark is a point of an object having some unique configuration and form with predefined properties which are uniquely identified only from some special position. The scan of such object gives some contour on the US image, and only several special points that are defined by phantom's construction are classified as landmarks.
- **Registration phantom.**
The phantom form is undefined, it may be almost any amorphous object made from any suitable material visible to the ultrasound and having some unique well detectable form. The phantom must be also well detectable by some another image modality (e.g. computer tomography or magnetic resonance imaging) because the idea of this phantom is to scan it with two different modalities and match both obtained datasets to each other. Theoretically all points obtained from a scan may be considered the landmarks, practically what points are selected for matching purpose depends on the data segmentation and matching algorithm, because datasets obtained from two different medical images modalities differ strongly and must be adjusted to each other.
- **Combined approaches** (e.g. plane phantom with wires).
Any workable combinations of the described landmarks. One of the possible solutions, the "Plane phantom with wires", is described in the state of the art.

2.4. Analysis of existing calibration techniques in application to UFASS calibration

No unified calibration phantom is invented by now. The huge quantity of calibration phantoms is caused by the fact that each calibration case may have different requirements that are fulfilled by one of the phantoms in one case and by totally different phantom in another case. In this section we analyse the standard calibration approaches in application to the calibration of the UFASS using the requirements formulated in the previous section.

2.4.1 Point phantoms

Single small objects like beads are the classical landmarks for calibration phantoms. They are very easy to construct and visible from any position since they are symmetrical. However, due to the physical properties of the ultrasound beam and the quality of ultrasound image modality, this type of landmarks require manual positioning of the US transducer for scanning and manual detection of the scanned bead on the image which makes it insufficient for our purposes.

The cross-wire phantom has similar properties as just beads, however it supports less positions and orientations since it may not be scanned from all directions. Its scanning and point detection procedure is a bit easier than for single points because additional wires provide tracking feedback, but it is still a manual procedure. Additionally it is not robust, as each phantom that uses wires is. These factors remove the cross-wire phantom from our candidates list.

Spherical landmarks support automatic image detection because a spherical object gives a clear detectable contour on the US image. It is classified as a point landmark because only the ball's centre – a single point – is taken for the calibration procedure. These landmarks are robust, cheap, and may be scanned from different positions and distances. The known problem for these landmarks is that a method to align the ultrasound beam with the ball's centre must be provided. Assuming that we may provide such a method this type of landmark can be taken for further examination.

Calibration with a stylus is also a manual one, which is inappropriate for our purposed. The transducer must be aligned with the stylus tip that requires some experts skills. Moreover, it requires to use an additional device which would increase the costs of each calibration phantom.

2.4.2 Wire phantoms

Wire phantoms are in general less robust than other phantoms. A thin wire can much more easily get deformed than for example a metal plane or a sphere. Nylon wires may be even deformed by the temperature, and since mostly warm water is used for calibration to simulate the speed of sound in the human tissues, wires seems in general not to satisfy the robustness criterion.

The three-wire phantom provides simple scanning procedure, however with the UFASS it does not seem to cover all possible positions. Manual detection on the US images is still required. It is also very fragile and requires a very precise construction since the three wires must be placed ideally orthogonal to each other.

Some of Z-phantom variations provide automatic landmarks detection procedure that is definitely an advantage that makes the whole procedure rather expert-independent. The costs of the phantom are normally not high. Production is however not easy, the main difficulty usually lies on measuring the wires geometry precisely. The other disadvantage is a limited range of positions from that the landmarks can be scanned. This is caused by the phantom geometry, where the landmarks wires are placed in one scanning plane which must be scanned from directions near to it's perpendicular.

Lack of robustness and scanning positions variety makes wire phantoms not suitable for further investigation.

2.4.3 Plane phantoms

The main advantage of the plane phantoms is that their landmarks can be automatically detected on the US image.

The single wall phantom is robust and very easy to construct but it is not precise due to the beam width problem. In it's standard implementation, where usually the bottom of the water tank or a surface of some flat object is taken, it does not support positions and orientation variety required by the UFASS because the plane must be scanned from the top in order to reduce the beam width problem, and the UFASS requires the 360 degrees view.

The Cambridge phantom is neither cheap nor simple, and requires some expert skills for usage. But it is a very precise calibration instrument and allows automatic image processing. However it is impossible to use it in the UFASS calibration because the Cambridge phantom requires to attach the ultrasound probe to a special clamp which is a part of the calibration phantom. In our scanner the probe position within the scanner is an integral part of the calibration process itself, that's why the probe may not be reattached and must be calibrated within the device.

2.4.4 Alignment phantoms

Alignment phantoms are reported to require very few scans (mainly even one is enough), but precise manual alignment of the ultrasound probe with phantom landmarks is required. This fact and manual, or in the best case half-automatic

2.4. Analysis of existing calibration techniques in application to UFASS calibration

image segmentation increases the calibration duration. It also makes these methods expert-dependent which is inappropriate for the UFASS calibration. Moreover, the idea of the alignment phantom is that its landmark should be scanned from one specific position, that contradicts with the requirement that the UFASS must support a variety of transducer positions and orientations. Both these facts exclude alignment phantoms from our research.

Stopping on further calibration objectives we must mention the advantages of the shape board, which are low costs, construction simplicity and robustness. Unfortunately they do not overcome the mentioned drawbacks in application to the UFASS calibration.

The mechanical instrument from Gee et al., even being a very precise calibration phantom, is inappropriate also from the same reasons as the Cambridge phantom. It requires to attach the US probe to it and is very complicated and expensive.

The last type of the alignment phantoms, the wedges phantom, is robust and not expensive but not accurate enough, since the reported accuracy is 1.6 mm RMS, which is much more than for other reviewed phantom, most of that have the accuracy lower than 1 mm RMS.

2.4.5 Registration phantoms

Registration phantoms do not have any specific design. This opens a large variety of phantom design configurations but also makes it difficult to analyse this type of phantom in general in application to the UFASS calibration. Those phantoms presented in the literature (see Section 1.3.5) are not ideally suitable for the UFASS from the perspective of distances and position varieties. Also the main drawback of registration phantoms is not very high accuracy – the highest was 0.83 mm RMS reported by Huang et al. [44]. This type of phantoms may also be taken into consideration in case if other landmarks do not show more promising results.

2.4.6 Other phantoms

Landmarks may also be combined within one phantom. One example of combination of a cross-wire phantom with a plane is reported by Dubouski et al. [28]. This phantom even provides an automatic landmarks detection procedure, but the alignment with the landmarks must be performed manually. The accuracy is also not very high (1.14 mm RMS).

2.4.7 Resume

Fulfilment of the UFASS calibration requirements by the listed standard calibration phantoms is concluded in the Table 2.1. The last column shows whether this type of phantom is considered suitable for further investigation.

From the point group the spherical landmarks are considered the most promising. Wire phantoms are not applicable for the UFASS because of either lack of scanning position varieties support or manual landmarks detection. A plane-based solution also suffers from the lack of positions and orientations, or is not applicable because requires the ultrasound probe to be reattached from the scanner. The alignment group is considered not suitable for the UFASS calibration due to manual data acquisition and detection procedure as well as the combined approach. The registration phantom has too low accuracy, but may be further investigated if other landmarks do not give results that overcome its accuracy.

After examining the existing calibration techniques we may say that a new phantom with a custom calibration procedure must be constructed to fulfil the formulated requirements. Our research resulting in constructing the multi-spheres phantom and the correspondent calibration procedure for the UFASS is described in the following chapter.

¹Robustness

²Low costs and construction simplicity

³Execution simplicity and speed

⁴Self-sufficiency and expert-independence

⁵Distances range support

⁶Positions and orientations variety support

⁷Automatic image processing

2.4. Analysis of existing calibration techniques in application to UFASS calibration

Requirements	Robust. ¹	Costs ²	Exec. ³	Exp. ⁴	Dist. ⁵	Pos. ⁶	Auto IP ⁷	Suitable
Point								
Beads	+	+	-	-	+	+	-	-
Spheres	+	+	+	+/-	+	+	+	+
Cross-Wire	-	+	-	-	-	+/-	-	-
Stylus	+	-	-	-	-	+	-	-
Wire								
Three-Wire	-	-	+	-	+	-	-	-
Z-phantom	-	-	+/-	+/-	-	-	+/-	-
Plane								
Single Wall	+	+	+	+/-	-	-	+	-
Cambridge	+	-	+	+/-	-	-	+	-
Alignment								
Shaped board	+	+	-	-	-	-	-	-
Gee et al.	+	-	-	-	-	-	-	-
Wedges	+	+/-	-	-	-	-	-	-
Registration								
Registration	?	?	+	-	?	?	?	?
Other								
Combined	+	+	+/-	+/-	-	-	+	-

Table 2.1: Fulfilment of the UFASS calibration objectives by standard calibration phantoms.

Chapter 3

The multi-spheres phantom for the UFASS calibration

Development of the calibration solution for the Ultrasound Fracture Analysis Scanning System started from the analysis of the calibration objectives of the system. Using the formulated requirements we analysed the standard state of the art calibration phantoms and stated that none of them fully satisfied the formulated calibration objectives. We selected the most promising class of phantoms landmarks – the spherical markers – and analysed them to state out that they are suitable for further investigation. After a series of tests we defined the phantom configuration and constructed the multi-spheres phantom. Afterwards we designed the new calibration procedure and the automatic landmarks scanning and US image detection method and implemented it in the calibration software. Finally we carried out tests to determine the accuracy of our procedure. We also performed calibration experiments with another calibration phantom and compared the results. As a conclusion for this research we analysed the advantages and drawbacks of our calibration procedure, it's possible applications for another automated diagnostics scanners, and possible improvements.

3.1 The multi-spheres phantom

To design a calibration phantom means not only to construct it, but to provide the complete calibration solution for the device based on this phantom. Designing a phantom includes the following steps:

- Select landmarks material and size.
- Specify phantom configuration – the number of landmarks and their positions and orientations.
- Define the calibration procedure for the UFASS using the new phantom.

- Construct the phantom.
- Perform calibration tests and analyse the results.
- Compare the provided calibration solution with another one (optionally).

3.1.1 Landmark

It was stated that a sphere is the most promising landmark type because it is robust, symmetrical and thus detectable from various positions and orientations. It provides a clear and easy, automatically detectable contour on an ultrasound image. Several research groups (see 1.3.1.2) successfully use spherical landmarks for phantom construction.

Though we use the word "landmark" for the whole sphere, actually only the sphere's centre is the point of interest that should be detected from the ultrasound scan. This centre point is treated as a standard point phantom for the calibration equations 1.1 and 1.2. Thus it should be possible to accurately detect the sphere's centre, that is a main criterion for the choice of the landmark which is taken into account in the experiments described in this section.

3.1.1.1 Choosing landmark material and size

A sphere imaged with a 2D ultrasound probe gives a circular shape on a B-scan. The circle's representation on an US image strongly depends on the ball's material. The ball should have a form of nearly a perfect sphere and should produce a clear accurate US echo.

For the material and size test we selected ten different small balls from 10 to 20 mm in diameter made from wood, rubber and different variants of plastic (see Fig.2 3.1). The size choice was naturally limited by scanner dimensions and the properties of the ultrasound beam. Larger spheres were too big for the scanner's inner basin. Also for the bigger spheres the full scan of it could not be achieved with the ultrasound transducer with some degree of freedom since the transducer is itself only 4 cm wide. Smaller spheres are more similar to beads, which were too small to provide a clear spherical contour on an ultrasound image, which contained much more image artefacts on surfaces with steep curvature.

For each ball we checked the following quality criterion: how well a circle of known diameter could be detected on the B-scan.

Balls 3.1a – 3.1d were wooden, 3.1e – 3.1g were from transparent plastic, 3.1h was metal in the rubber cover, 3.1i – 3.1j were from dense, non-transparent plastic.

For this test we made a B-scan of each ball passing through its centre. On each image we automatically detected the circle's centre by matching a known

3.1. The multi-spheres phantom

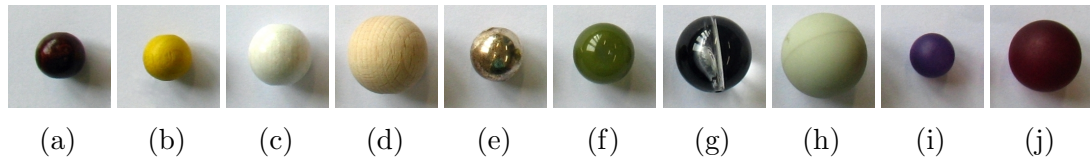


Figure 3.1: Balls for the landmark material and size selection test.

diameter circle template to the US image where best fit corresponded to the minimal cross correlation between the model and the data. The diameter of each ball was premeasured with a caliper. The results are presented on the Fig. 3.2. Some of the balls however didn't give sufficiently clear circle to provide the acceptable recognition results. All scans were taken at the same ultrasound settings to make the results comparable, because changing some imaging parameters may sometimes considerably change the displayed echo.

Since the real circle centre coordinates in this test were unknown, we performed the results comparison manually. It is known that due to the ultrasound modality properties the border of the scanned objects appears as a thick boundary rather than a thin curve. The thickness of the boundary depends on the scanned object material, moreover it is affected by various distortions and artefacts. However it is known, that the top most border point on the image belongs to the object because the US beam is straightly reflected from the object's surface at this point. We used this fact as well as the overall circle clearness as a detection quality criterion. When a similar result took place for a pair of comparable balls, we preferred one having a thinner contour. After this experiment we considered the matt non-transparent plastic balls 3.2i ($\varnothing 16$ mm) and 3.2j ($\varnothing 20$ mm) the most satisfactory, while wooden balls gave too thick contours, and transparent or reflective plastic did not give a circle shape. A metal-rubber ball seemed to have even a better US echo than the selected plastic ones, but it was too heavy for the purpose of stable phantom construction. Fig. 3.3 shows standard B-scans of the chosen balls.

3.1.1.2 Ball's centre detection in a series of sequential parallel US slices

The UFASS is equipped with two transducers. One of them is places horizontally, i.e. the scan plane is parallel to the scanner's bottom surface, and it's motion curve is a line from the bottom to the top of the water basin within the scanner. This transducer allows to obtain parallel B-scans in elevation direction with 0.01 mm accuracy.

The experiment described in this section was intended to answer the question: how well a scan correspondent to the ball's centre can be detected from a series

Chapter 3. The multi-spheres phantom for the UFASS calibration

of sequential parallel US slices made with this transducer? Parallel slices are obtained when the ultrasound probe is swept along the ball perpendicular to its axis taking the US images of the parallel sections. When a B-scan correspondent to the ball's centre can be recognized from such a sequence of images it means that the ball's centre can be later detected from this scan (given a working circle detection algorithm).

The experiment we performed consisted of two parts:

- Ball's centre detection with unknown diameter.
- Ball's centre detection with known diameter.

For the experiment we obtained five datasets with sequential parallel scans of a ball 10mm in diameter, each dataset contained 100 to 110 images. The ball was fixed in a clamp which was aligned with the transducer start position that way, that the first and the last scans contained no object, and the scans inbetween presented the ball's sections starting from one pole, and going through the centre to another pole. All scans were obtained with a parallel transducer shift by 0.1 mm. The position of the central slice was known from the clamp settings. These settings defined what coordinates did the ball's poles and central points have. The purpose of both experiments was to detect the B-scan correspondent to the central ball's section without preliminary information about the ball position, analysing only the data from the US images.

The purpose of the first part of the experiment was to check whether centre detection can be done without preliminary information about the ball's size and thereby avoid the measurement error. For each scan we applied a circle detection algorithm (described in 3.1.1.1) with various circle templates to detect a circle that best fitted the image. Since all scans had the same elevation distance between each other, the centres of the detected circles should formed a line in 3D space because all they lied on the ball's axis. At the same time circles diameters from each scan should formed a smooth curve with its maximum correspondent to the central scan. However, the results showed that the quality of the US image did not let us to obtain sufficient recognition quality. The algorithm gave a 8 percent error for the circle diameter and inconsistent positions of centres for each scan (see Fig. 3.4).

In the seconds part of the experiment the ball's diameter was considered a known value. For the same datasets we matched the template circle with the ball's diameter to the series of the B-scans. The slice best fitting the template was considered to be the central. For three datasets the slice found by the algorithm was the same as chosen manually, for the other two the next neighbourhood slice was found. Since the distance between two slices is only 0.1 mm this variation lies within the acceptable inaccuracy. We considered the described technique of a ball's centre detection with known diameter acceptable for further research.

3.1. The multi-spheres phantom

It should be mentioned that this algorithm always has a minimal centre detection error that depend on the distance between two parallel scans. Since the position of the ball is arbitrary, it can happen that no scans pass through the ball central section that is positioned between two neighbourhood central B-scans. In this case we have a centre detection error that is linearly dependent on the step between two slices, maximum the half of the scanning step. For our transducer this is 0.05 mm for the minimal possible scanning step.

Taking a smaller scanning step reduces the misdetection. Taking the larger step increases the scanning time, however we do not recommend it to avoid this error. It must be mentioned, that since the scanner is equipped with mechanical transducer positional system, theoretically even many scans of the landmark can be made without significant time consume. However practically the scanning procedure is performed in water, and moving the transducer too fast would produce waves. This is undesirable because water fluctuation would cause micro movements of the phantom even if it is solidly fastened within the UFASS. Also the picture of the ball surface may be changed due to the small bubbles that are formed on it's surface caused by water movements. That's why moving the transducer from one position to another must takes some fixed minimal amount of time, therefore the number of scans can not be increased limitless. In our experiment we use 100 to 110 scans for each ball. The system must contain at least six landmarks to solve the calibration equation (in practice 50 to 100 percent more landmarks are taken in order to increase the accuracy). This results in several hundreds of scans, which is inappropriate since it is very time consuming. That's why we recommend to scan only a middle part of the ball which is closer to the center. We repeated the experiment taking only middle 20 scans and the results were the same. Such prepositioning of a ball is possible because the UFASS may be programmed to position the scanner at any place, and if the phantom form is known, the starting position for each scan can be preprogrammed so that it is located in the area closed to the balls centres.

3.1.1.3 Ball's centre detection in a series of sequential angular US slices

In the previous experiment we examined the horizontally placed transducer of the UFASS, which is swepted along the ball's axis and provides the images of the ball's parallel slices. In this section we consider the second UFASS transducer, the vertically placed one. It provides the B-scans that image plane is parallel to the vertical axis of the scanner. The ultrasound probe is positioned in such a way that it is rotated around the main scanner's vertical axis and it's motion curve is a circle. For this positioning the ball is "cutted" into angular pieces by the scanning planes rather than being divided into parallel slices (see Fig. 3.5a). In a sequence of such angular images there may be none passing directly through the

Chapter 3. The multi-spheres phantom for the UFASS calibration

ball's center. This opens the following question: how does the centre detection error depend on the scanning procedure?

Let's say the transducer's rotation angle step is α and the distance between the ball's centre and the transducer is R . The worst case for centre detection is when the scan that passes through the ball's centre should be directly in the middle between two neighbour slices that are passing to the both sides of the centre. This means we should find how big the error for the angle $\alpha/2$ is, which is $\varepsilon = R \cdot \sin(\alpha/2)$ (see Fig. 3.5b).

To choose a proper phantom construction we need to determine possible distances from the balls to a transducer and to figure out the scanning angle step. Figures 3.6, 3.7 and table 3.1 show the ε error value depending on the α and R . Fixing an error threshold we can select allowed value pairs (α, R) from the table (cells marked with light grey). For our experiment we assumed a threshold equal to 0.2 mm as acceptable. From the table we see that for the maximal distance taken in the experiment (130 mm) an angle step less or equal to 0.18 degrees should be taken.

Since the radius of the UFASS is not larger than 100 mm we even may either take the larger angle step 0.23 degrees to achieve the same accuracy, or to take the smallest supportable rotation angle (rotation accuracy of 0.1 degree is supported) and get even smaller accuracy error (0.087 mm). Both cases are fully satisfactory, we consider this algorithm suitable for the ball's centre detection for the UFASS.

3.1. The multi-spheres phantom

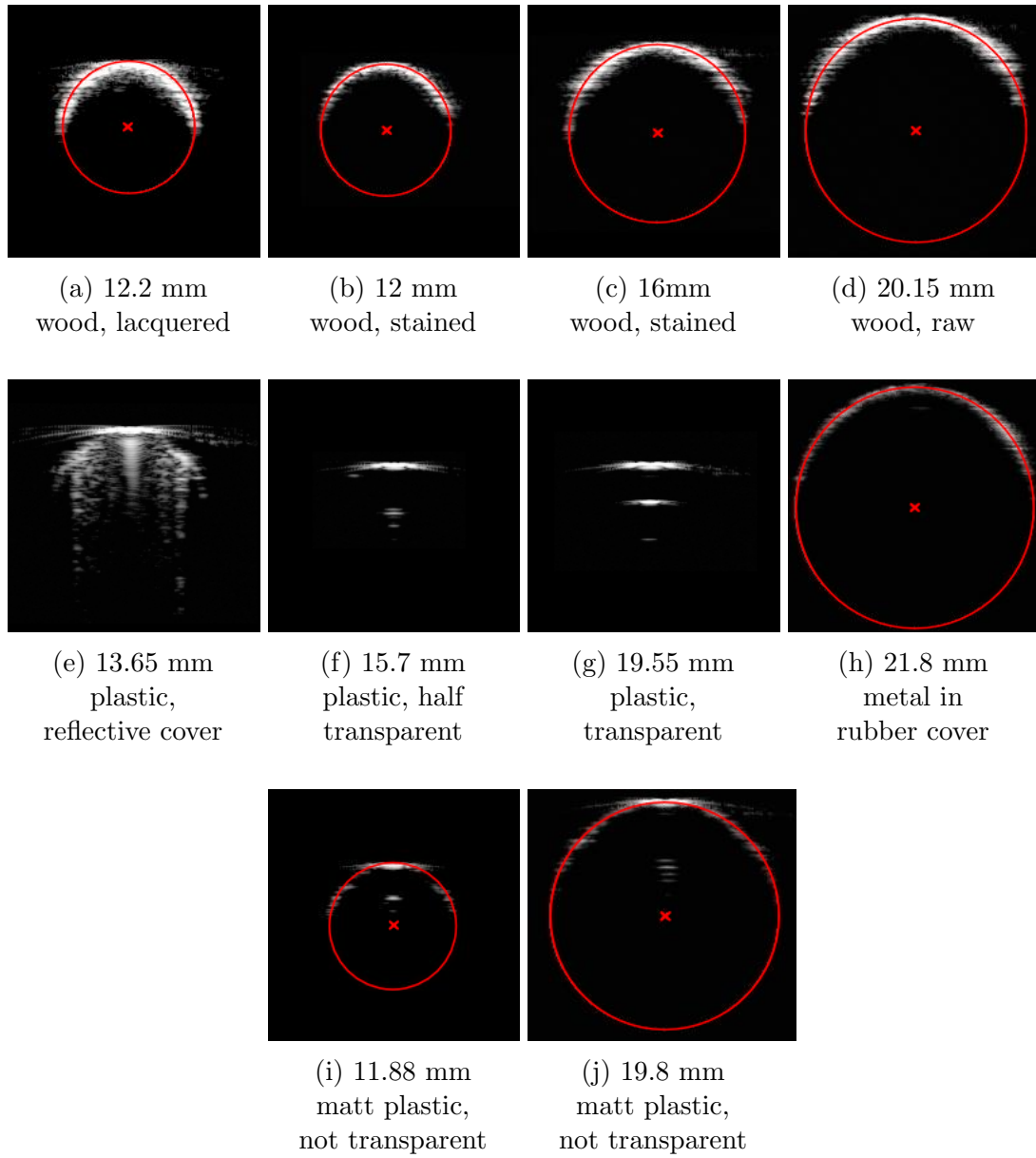
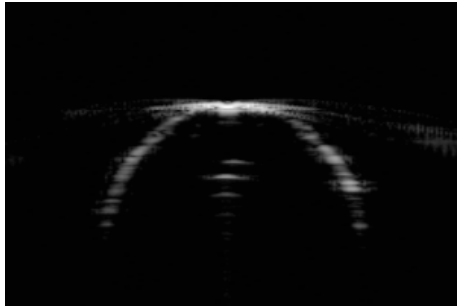
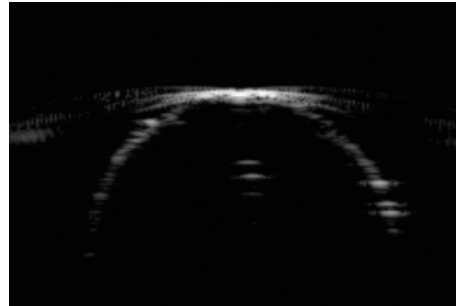


Figure 3.2: Circles detection on the B-scans.

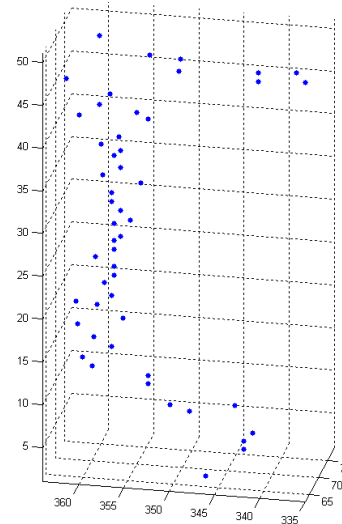


(a) Ball 3.1i.



(b) Ball 3.1j.

Figure 3.3: Standard B-scan for the chosen plastic balls.



(a) Circle diameter depending on the slice number. (b) Circle centers for each slice.

Figure 3.4: Ball's centre detection with unknown diameter.

3.1. The multi-spheres phantom

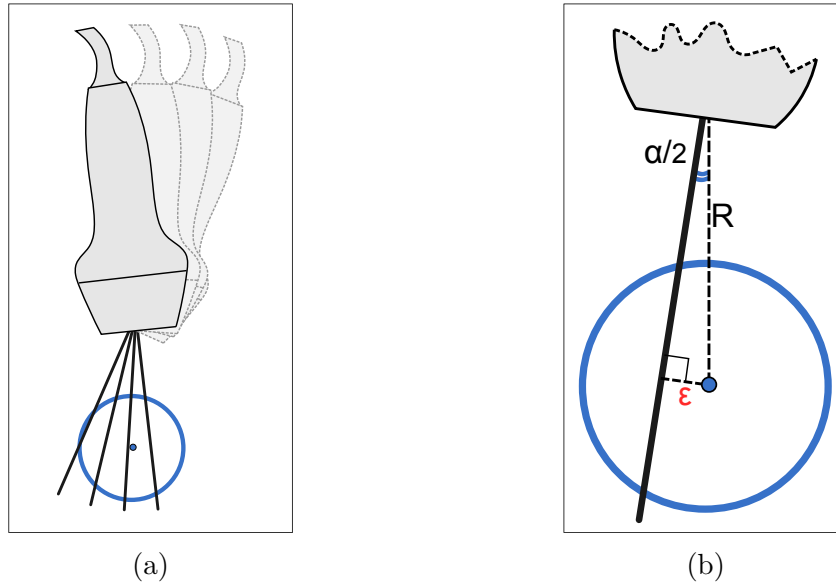


Figure 3.5: US beam trajectory for a transducer rotated around the ball's axis. 3.5a: An US beam can pass not directly through a ball's centre. 3.5b: An error ϵ of centre location with the beam angular deflection of $\alpha/2$ and the R distance from the transducer to the ball's centre.

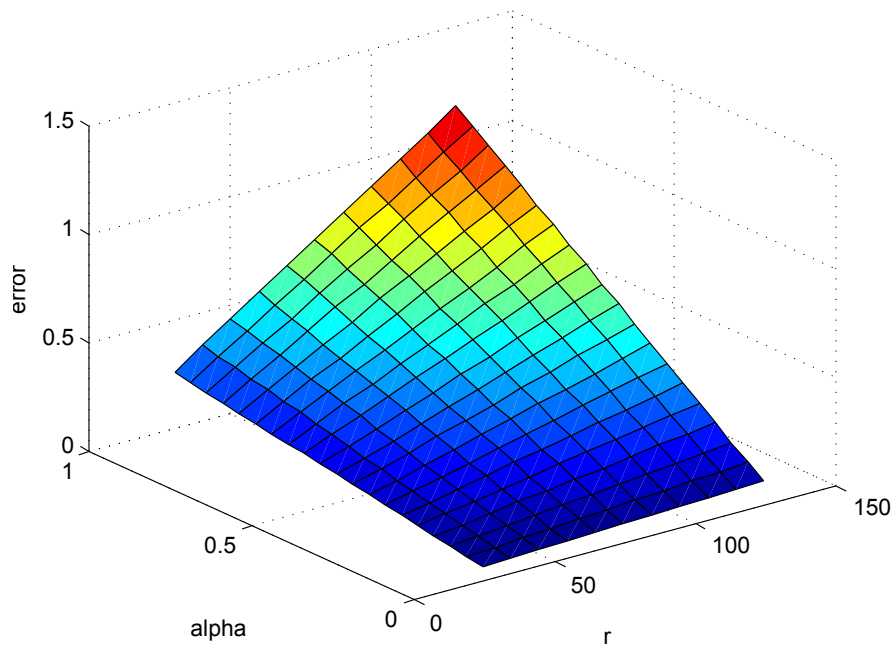


Figure 3.6: Centre detection error for a transducer rotated around the ball's axis. A surface shows the error value ϵ depending on the rotation angle step α (in degrees) and the distance R (in mm) from the transducer to the ball's centre.

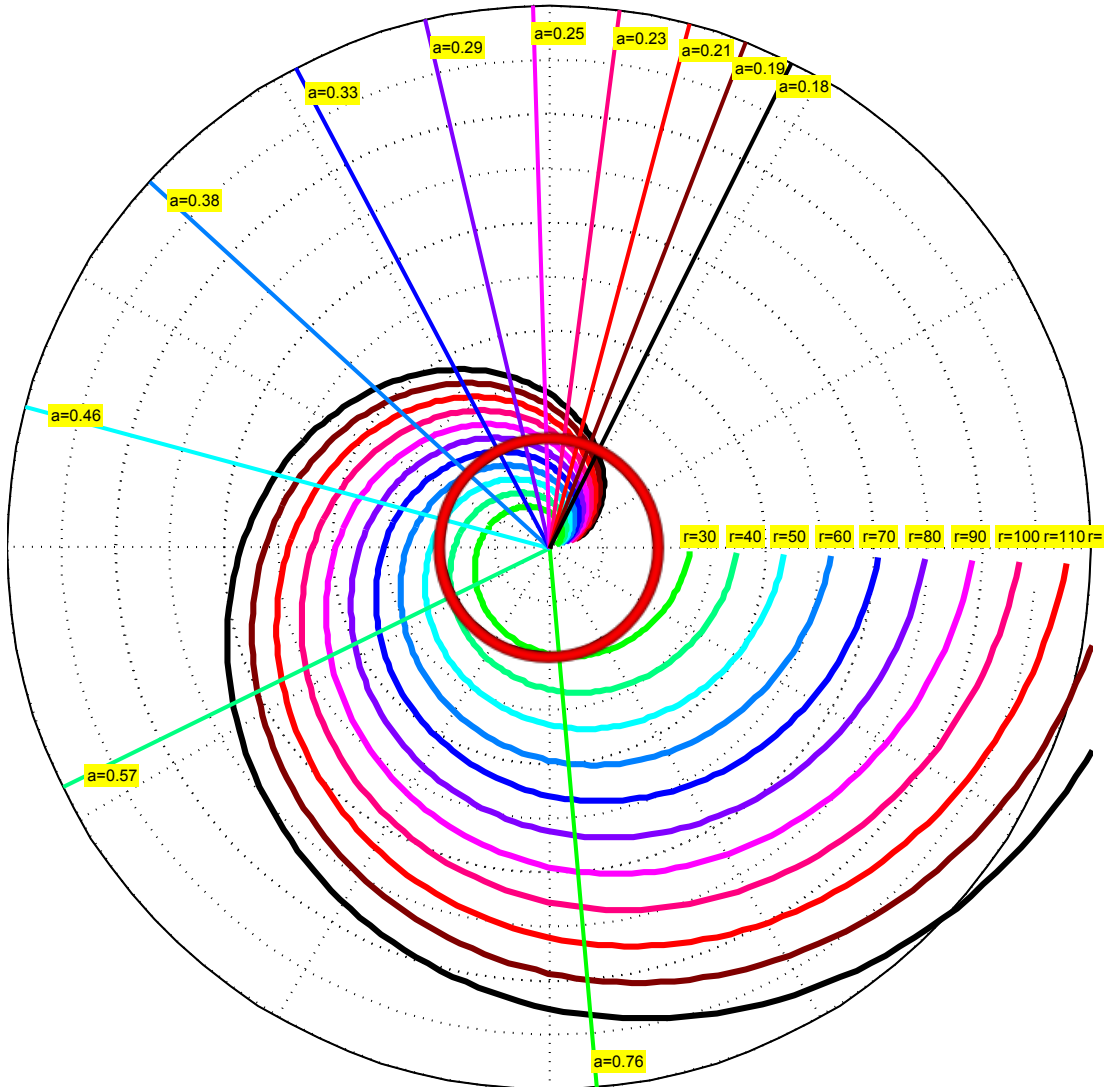


Figure 3.7: Centre detection error for a transducer rotated around the ball's axis. Each spiral curve shows the error value ε depending on the rotation angle step α (in degrees, each α value corresponds to one circle) for a fixed distance R (in mm) from the transducer to the ball's centre. A red circle represents the error threshold (0.2 mm) which is selected as the highest acceptable value for this experiment. Straight coloured lines correspondent to each curve show the α value at which this threshold is achieved for the fixed R value. Each values pair (α, R) inside the red circle is permitted for the experiment.

3.1. The multi-spheres phantom

$\alpha \backslash r$.05	.1	.15	.2	.25	.3	.35	.4	.45	.5	.55	.6	.65	.7	.75	.8	.85	.9	.95	1
30	.013	.026	.039	.052	.065	.078	.092	.105	.118	.131	.144	.157	.170	.183	.197	.209	.223	.236	.249	.262
40	.017	.035	.052	.070	.087	.105	.122	.140	.157	.175	.192	.210	.227	.244	.262	.279	.297	.314	.332	.349
50	.022	.043	.065	.087	.109	.131	.153	.175	.196	.218	.240	.262	.284	.305	.327	.349	.371	.393	.415	.463
60	.026	.052	.078	.105	.131	.157	.183	.209	.236	.262	.288	.314	.340	.367	.393	.419	.445	.471	.498	.524
70	.031	.061	.092	.122	.153	.183	.214	.244	.275	.305	.336	.367	.397	.428	.458	.489	.519	.550	.580	.611
80	.035	.070	.105	.140	.175	.209	.244	.279	.314	.349	.384	.419	.454	.489	.524	.559	.593	.629	.663	.698
90	.039	.078	.118	.157	.196	.236	.275	.314	.353	.393	.432	.471	.511	.550	.589	.628	.668	.707	.746	.785
100	.044	.087	.131	.175	.212	.262	.305	.349	.393	.436	.480	.524	.567	.611	.655	.698	.742	.785	.829	.873
110	.048	.096	.144	.192	.240	.288	.336	.384	.432	.480	.528	.576	.624	.672	.720	.768	.816	.864	.912	.960
120	.052	.105	.157	.201	.262	.314	.367	.419	.471	.524	.576	.628	.681	.733	.785	.837	.890	.943	.995	1.047
130	.057	.113	.170	.227	.284	.340	.397	.454	.510	.567	.624	.681	.737	.794	.851	.908	.964	1.021	1.078	1.134

Table 3.1: Error of centre detection for a transducer rotated around the ball's axis, depending on the scanning angle step. Cells marked with gray correspond to the value pair (α, R) which are acceptable for the experiment assuming the error threshold equal to 0.2 mm.

3.1.1.4 Ball's centre detection accuracy

In the previous sections we checked the hardware errors, i.e. the measurement errors unavoidable because of the scanner construction. In this section we checked the total error of the ball's centre detection, which showed the accuracy of a spherical landmark detection.

For this experiment it was necessary to know the real centre coordinates in the 3D space. For this purpose we fixed a ball on a simple parallelepiped metal plane with known dimensions and measured the ball's position relative to the metal surface with a caliper as shown on Fig. 3.8a.

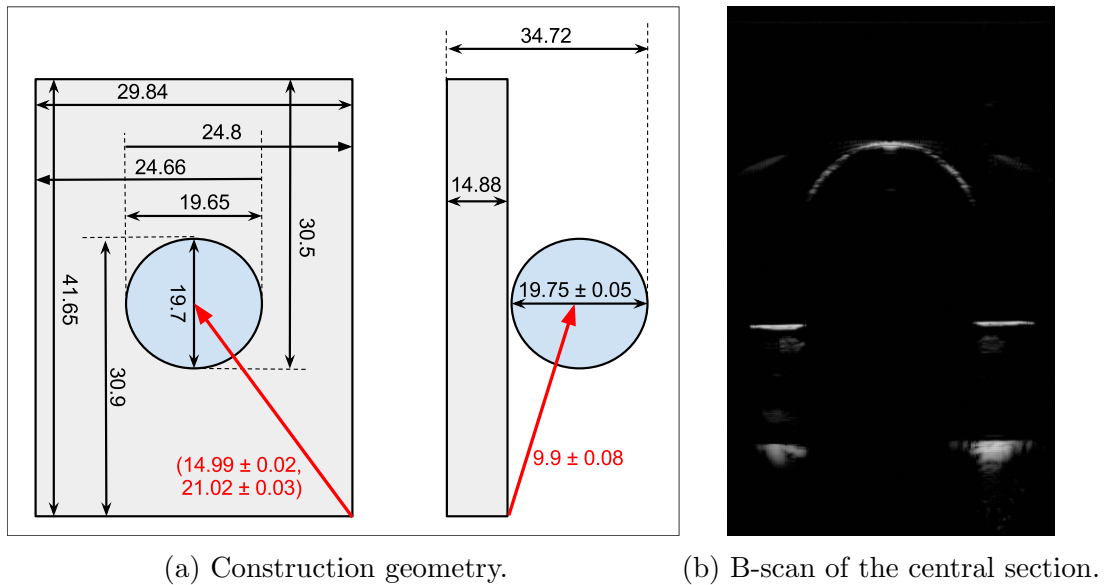


Figure 3.8: Ball's centre detection from a series of images. A known-size object with a ball on it gives a B-scan on which both the ball's circle section and the metal surface under the ball can be detected.

We obtained a series of B-scans of the ball with the underlying metal plane with 0.1 mm step between the slices. The metal plane gave a strong easily detected reflection though it's position could be automatically detected. We considered one corner of the shape to be the coordinate system centre, and measured the distance from it to the ball's centre. Then, from a series of US images we got the B-scan correspondent to the ball's central section (as described in 3.1.1.2) and detected the circle's centre on this image. As a reference we manually selected a B-scan with the shape's corner representing the coordinate system centre and detected this point. For both geometrical measurements and the US data we calculated and compared the distance between the ball's centre and the selected coordinate system centre. The centre detection error from this experiment was

3.1. The multi-spheres phantom

(by X , Y and Z correspondingly):

$$(0.41 \pm 0.02, 0.115 \pm 0.08, 0.38 \pm 0.03) \quad mm$$

This means that an error less than **0.5** mm is achievable for a single ball's centre detection which is satisfactory for the phantom construction. Many state of the art phantoms have accuracy more than 1 mm, and only few of the phantoms lie below the 0.5 mm border.

3.1.2 Choosing phantom geometry

After we checked that a spherical landmark is an appropriate landmark for our phantom, we had to define the phantom configuration, i.e. the quantity and the positions of the spheres.

Landmarks quantity. According to the calibration equations 1.1 and 1.2 at least six data points are required to solve the calibration equation and obtain the calibration matrix. However in practice at least 50 percent more points are normally taken to improve the accuracy. As stated in the previous section it is necessary to keep the landmarks quantity low in order to shorten the scanning time. The reason is water fluctuations caused by the scanner movements, which should be reduced to minimum. That's why we tested the configurations consisting of 10 to 18 spheres, i.e. from 50 percent + 1 sphere to 300 percent of the minimal required landmarks quantity.

Landmarks position. It was stated that for the vertically placed transducer of the UFASS the less the distance from the ball to the scanner is the higher the accuracy is. Furthermore, the landmarks must be placed that way, that they are visible from all possible positions and orientations of the scanner. That is one of the UFASS calibration requirements, which is necessary to provide the accurate calibration from all directions. We already stated that there should be several balls in the phantom, and the most natural way would be to place them on the circular curve repeating the vertical transducer movement trajectory. To support the other calibration requirement - different scanning depths, i.e. the distances from the landmark to the scanner, the landmarks should be positioned not directly onto the circular curve, but with some diversity. Since there is also the horizontally placed transducer in the scanner, which trajectory is a line parallel to the vertical axis, the landmarks should be placed on different heights in order to cover the full heights variety.

For the suggested configuration we selected the following construction for our phantom: several balls should be attached with horizontal thin bars to a central thick vertical bar. Each horizontal bar has different length and is rotated on some angle around the main bar. Such a construction allows the calibration to be hold on different depths and heights if the phantom is placed into the scanner

Chapter 3. The multi-spheres phantom for the UFASS calibration

central point so that the main vertical bar is aligned with the scanner rotation axis. This construction provides several variations, e.g. different lengths and orientations of the horizontal bars. We simulated and theoretically tested three possible phantom configurations which fulfilled this basic conception to figure out, whether some of them had certain advantages (see the models on Fig. 3.9).

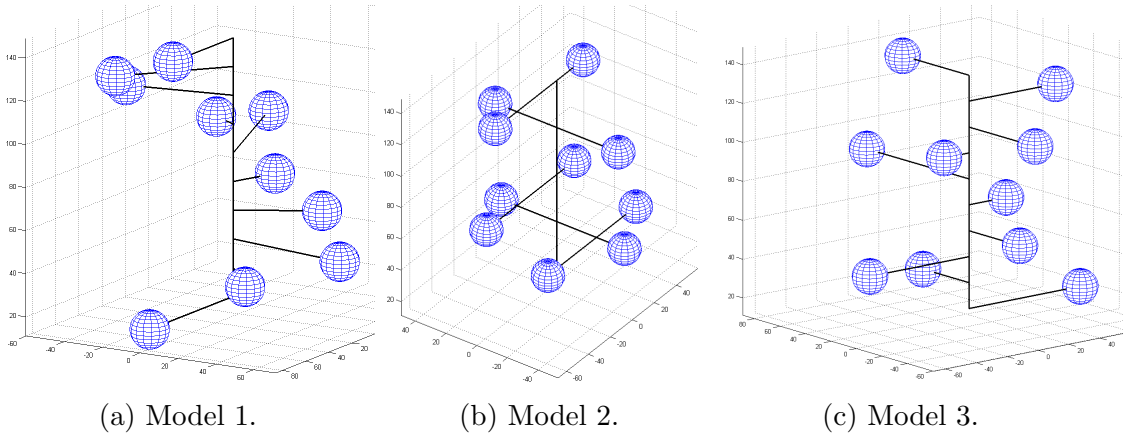


Figure 3.9: Possible phantom configurations. First model has higher variety of angles ($0^\circ, 36^\circ, 72^\circ, 108^\circ, 144^\circ, 180^\circ, 216^\circ, 252^\circ, 288^\circ, 324^\circ$), one ball at each height. Second model has two balls at each height, fewer height levels at four angles ($0^\circ, 90^\circ, 180^\circ, 270^\circ$). Third model has one ball per height level at four angles ($0^\circ, 90^\circ, 180^\circ, 270^\circ$).

We simulated each model for different balls quantity (from 10 to 18). For each case we obtained the artificial calibration data using real scanner dimensions and supposed scanning protocol. A random error from 0.3 to 1 mm has been added to the data to simulate possible measurement and ball's centre detection errors. With this data we performed a calibration procedure for each model configuration 10 times (each time with different randomness) and calculated the mean result error. For a single calibration an error was calculated as a distance RMS (euclidean distance between the real ball's centre and the centre obtained from the simulated US data transformed using the obtained calibration matrix). Results for each model are presented in the tables 3.2, 3.3 and 3.4 (model 2 has always two balls of each bar that's why only even balls quantity are tested).

According to these results we assume that a calibration error from 0.2 mm to 0.8 mm is feasible when data acquisition error is between 0.3 and 1 mm. For the most experiments the calibration error grows slightly when the ball's quantity increases that lies on the relatively high data acquisition error. There is no significant difference between three models, so we conclude that a model easiest in construction and scanning should be chosen. We suggest to use 12 landmarks because the total length of the phantom with them is approximately the same as the scanner's inner part. This quantity would cover all the possible heights

3.1. The multi-spheres phantom

Balls Quantity	Maximal Randomness Error	0.3	0.4	0.5	0.6	0.7	0.8	0.9	1.0
	10		0.1843	0.2410	0.3215	0.3965	0.4188	0.5034	0.5149
11		0.1837	0.2507	0.3167	0.3839	0.4287	0.5261	0.6123	0.6560
12		0.1988	0.2440	0.3223	0.3806	0.4555	0.5523	0.5846	0.6490
13		0.1982	0.2759	0.3496	0.4265	0.4929	0.5439	0.5582	0.6289
14		0.1951	0.2844	0.3289	0.3874	0.4194	0.5292	0.6213	0.6884
15		0.1937	0.2783	0.3378	0.4267	0.4875	0.5612	0.5969	0.7145
16		0.2102	0.2943	0.3481	0.4054	0.5256	0.5515	0.6392	0.6591
17		0.2119	0.2733	0.3524	0.4282	0.5238	0.5713	0.6771	0.6694
18		0.2158	0.2819	0.3646	0.4387	0.4916	0.5559	0.6337	0.6947

Table 3.2: Phantom Model 1 simulation. Calibration error depending on the ball's quantity and maximal value of the random error in the calibration data.

Balls Quantity	Maximal Randomness Error	0.3	0.4	0.5	0.6	0.7	0.8	0.9	1.0
	10		0.1634	0.2502	0.3005	0.3822	0.3952	0.4743	0.5311
12		0.1890	0.2542	0.3288	0.3779	0.4550	0.5492	0.6014	0.6641
14		0.2080	0.2360	0.3505	0.3989	0.4893	0.5521	0.5979	0.7318
16		0.2151	0.2743	0.3643	0.4173	0.4828	0.5472	0.6208	0.7174
18		0.2153	0.2813	0.3449	0.4415	0.5187	0.5878	0.6528	0.6992

Table 3.3: Phantom Model 2 simulation. Calibration error depending on the ball's quantity and maximal value of the random error in the calibration data.

Balls Quantity	Maximal Randomness Error	0.3	0.4	0.5	0.6	0.7	0.8	0.9	1.0
	10		0.2006	0.2705	0.3212	0.3682	0.4525	0.5281	0.5058
11		0.1933	0.2594	0.3092	0.3666	0.4776	0.5156	0.5189	0.6549
12		0.1925	0.2614	0.3169	0.3818	0.4613	0.5386	0.5905	0.6961
13		0.2032	0.2786	0.3275	0.4106	0.4884	0.5385	0.6099	0.6690
14		0.2105	0.2741	0.3533	0.4120	0.5144	0.5258	0.6673	0.6798
15		0.2035	0.2688	0.3505	0.4085	0.4953	0.5281	0.6205	0.6727
16		0.2113	0.2733	0.3515	0.4013	0.4946	0.5364	0.6309	0.6988
17		0.2113	0.2813	0.3395	0.4183	0.5004	0.5743	0.6412	0.7214
18		0.2157	0.2876	0.3744	0.4240	0.5087	0.5582	0.6595	0.7253

Table 3.4: Phantom Model 3 simulation. Calibration error depending on the ball's quantity and maximal value of the random error in the calibration data.

of the transducer. Since less balls quantity do not necessarily decreases the total calibration error, by demand only some subset of the landmarks can be used for the calibration which increases the flexibility of the calibration procedure.

3.1.3 Phantom design

Induced by the UFASS calibration objectives and the test results described above we constructed a multi-spheres phantom (see Fig. 3.10) that consists of the following parts:

- 12 landmarks, each one represented by a centre of a plastic ball of two different sizes: $\varnothing 16$ mm or $\varnothing 20$ mm. Each ball has a unique height location (the distance between each two neighbours is 10 mm) and one of the four possible orientations (each one is rotated on 90° relatively to it's neighbour around the central phantom axis).
- Phantom coordinate system marks. We implemented these marks as 5 small dots pricked on a thin aluminium plate. The plate is attached to the top of the phantom. A method that defines the phantom coordinate system using these dots is described later.
- Marker balls arrangement and fixation parts. Each ball is fixed on a thin ($\varnothing 5$ mm) steel bar that is attached to one central thick pole in a unique height position. The length of each bar is unique as well and is within the range of 30 – 70 mm. The central bar is made from aluminium and is $\varnothing 20$ mm. These parts are not crucial for the phantom construction and may be constructed in another way provided that visibility and accessibility of the landmarks for the scanner remain the same.

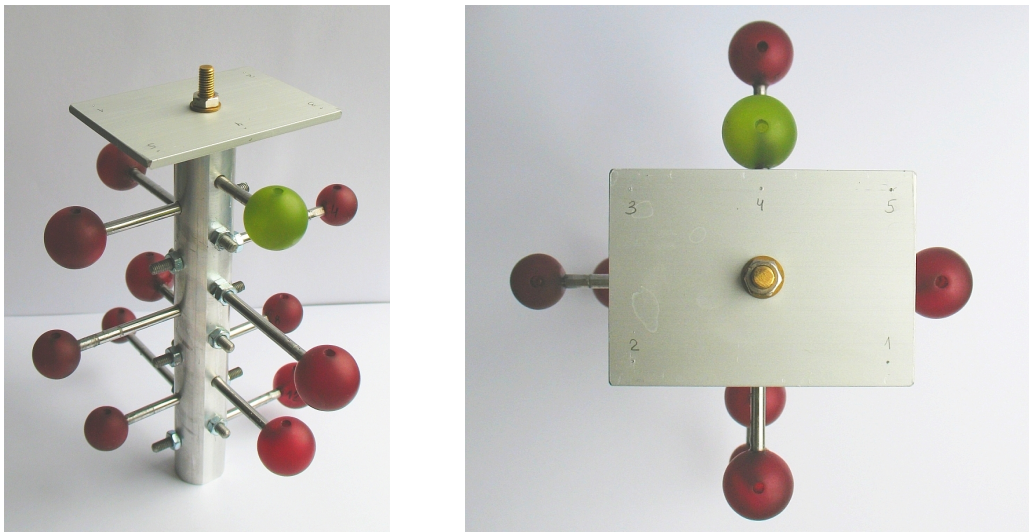


Figure 3.10: The multi-spheres phantom.

3.1. The multi-spheres phantom

This construction provides certain flexibility in the calibration procedure since not all of the 12 balls are obligatory to scan. From the whole set a subset of 6 or more balls may be selected which is enough for the calibration. Selecting less balls or only those lying in the region of scan interest may shorten the calibration procedure.

3.1.4 Phantom model

Building a phantom model is the preliminary stage in the calibration process. To carry out the calibration with the multi-spheres phantom it's reference model should be built. This model provides us with the reference landmark coordinates, that – during every calibration procedure – are matched with the acquired US data.

For the following experiments we obtained and compared two phantom models:

- **Pointer model.** Each marker ball was measured from different positions and orientation with the MicroScribe digital localizer (see Appendix) 25 times. Five coordinate marks were measured 5 times each and used to define the phantom coordinate system. The balls were approximated with spheres using the obtained points lying on the surface. The sphere's centres denoted in the phantom coordinate system coordinates were considered the reference landmarks.
- **CT model.** A CT volume of the phantom was obtained with the 0.38 x 0.38 x 0.6 mm resolution. Marker balls and coordinate system marks positions were detected from the images. Similarly to the Pointer model balls centres were calculated and expressed in the phantom coordinate system. However, there was one significant difference that influences the result model quality. Since the phantom was made mostly from steel and aluminium, the CT modality gave a lot of bright artefacts that complicated phantom edges detection on the US images. It resulted in a less accurate model which led to a higher calibration error.

3.1.5 Scanner calibration

In this part our calibration method designed for the UFASS calibration with the multi-spheres phantom is described.

For the calibration we use the standard notation described by the equation (1.1) that involves the following coordinate systems:

- *I*: US image coordinate system.
- *P*: position sensor coordinate system which we also call "tracking system".

UFASS has no external position sensor but a built-in system that tracks probe movements. P centre is in the rotation centre of the scanner, Z -axis of the system is coincided with the elevation direction and is also referred as the scanner axis. Scanner transducers have 4 DOF: rotation around the scanner axis, translation along this axis, changing the probe orientation around the "probe – scanner axis" direction and translation along it.

- S : scanner coordinate system. This system coincides with the system P with zero rotation and elevation values.
- G : global coordinate system that is represented by the phantom system in our solution. It is defined by three point marks on the phantom top. One point acts as the system centre, the second defines the X axis and the third defines the half-plane where the Y axis positive direction lies.

In this notation coordinate system matrices in the calibration equation (1.1) have the following meaning:

- $T_{P \leftarrow I}$: unknown calibration matrix (the goal of the scanner calibration task).
- $T_{S \leftarrow P}$: matrix describing the probe holder's position within the scanner. Consists of the elevation translation and rotation obtained from the scanner position controller.
- $T_{G \leftarrow S}$: matrix describing the phantom position within the scanner. For the prototype UFASS scanner that we have used in our experiments this matrix is unknown, we describe the way to obtain it below. However in the production version of the scanner it would be a known matrix since there would be a rigid holder provided to fixate the phantom in a way, that it's position relative to the scanner body remains the same.

For the scanner calibration the phantom is attached to a holder and located in the scanner. Next, the following calibration procedure takes place.

- **Scanner – Phantom transformation determination.**

This is a step that would be skipped in the non-prototype production scanner. The $T_{G \leftarrow S}$ transformation would be calculated only once after the scanner has been constructed. By each of the following calibrations the phantom would be attached to the scanner's holder invariably because the rigid holder does not provide any variation for the phantom position.

In the prototype device in order to obtain the matrix $T_{G \leftarrow S}$ we should measure the phantom coordinate system position and the scanner coordinate system position with some external measuring device and then calculate the transformation from one system to another. To obtain the Scanner – Phantom transformation we used the MicroScribe spatial localizer because of it's simplicity and low costs. This procedure is fast (takes approximately one minute) and does not require any special experience from a user. The

3.1. The multi-spheres phantom

measurement consists in touching the five points of the top of the phantom and the five points on the top of the UFASS prototype with the sharp top of the localizer. In general, three points are enough to define a coordinate system under condition that the measurements are precise enough. We propose to use two additional control points for coordinate system definition to increase the accuracy. Firstly, with the localiser we measure five phantom coordinate marks: correspond to a central point, to X and Y axis directions, and to control points defining the XY plane. Each measurement is repeated five times and the average value is taken. These five points define the phantom coordinate system. The scanner coordinate system position is obtained in the similar way. With these points the transformation from one coordinate system to another is automatically calculated that gives us the $T_{G \leftarrow S}$.

This procedure can be also done automatically if a position detection camera is available. In this case optical markers should be attached both to the scanner and to the phantom, then the camera should be used to obtain their coordinates which is performed in an automatic way.

- **Data acquisition.**

On this step we collect a set of ultrasound images for each of the phantom landmarks. Each landmark's coordinates are detected from that B-scan in a set of scans that better fits the central ball's section (see the next calibration step). Each marker ball is scanned several times from a number of neighbour US probe positions forming a trajectory that should pass near the ball's central section as close as possible. For the horizontally placed transducer this is a line providing a set of parallel slices, for the vertically placed transducer this is a set of angular slices (see Fig. 3.11)). The common requirement is to set up a small distance step between the scans in the sequence. The step size directly affects the centre location error, e.g. for the sequence of parallel scans the maximum error is a half of the distance between scan pairs. We use 21-scans sets with the 0.1 mm moving step.

The described procedure is repeated for various probe initial positions that results in several datasets per ball (for our experiments we took 5 datasets to increase the accuracy). Transformation matrices defining the transducer position correspondent to the B-scans are stored and used for the calculation of the result 3D coordinates. For the used UFASS prototype we perform the probe translation and rotation movements for data acquisition half-automatically. The rotation and translation mechanisms are integrated into the prototype scanner, but the motors are not attached, that's why one must manually rotate the steering wheel to initiate the transducers movements. However, for the final device with motors the whole procedure can be programmed and executed fully automatically.

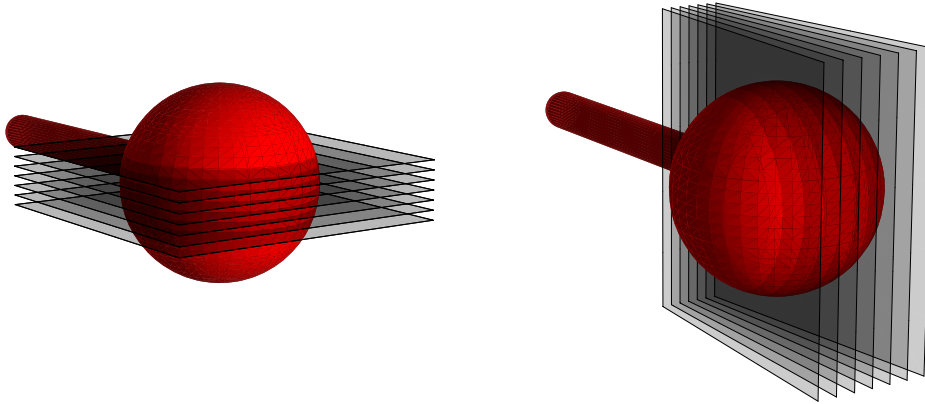


Figure 3.11: Multi-spheres phantom data acquisition for parallel and angular scanning procedure.

- **Landmarks detection.**

A dataset collected for each of the marker balls on the previous step consists of several B-scans with a part of a circumference representing the ball's section. To find the scan that better corresponds to the real ball's centre we run a circle detection algorithm based on the cross-correlation. The algorithm matches a circle with known radius to each image and selects the highest cross-correlation value as the central section. The centre of the detected circle on this section is a landmark point for the current marker ball.

- **Calibration matrix calculation.**

The last step of the calibration procedure is implemented as an optimization algorithm minimizing the distance function between the phantom model and ultrasound data. Points p_I in equation (1.2) are the landmark coordinates from the previous step multiplied onto the scaling coefficients s_x and s_y . These scalings translate pixel values to millimetres. Reference points p_G are taken from the model. The system of linear equations (1.1) is solved using the Levenberg-Marquardt algorithm. As a result we obtain the calibration matrix $T_{P \leftarrow I}$.

We have provided the detailed description of each calibration step, however most of these steps would be invisible to the final user and would be performed with the calibration software that was implemented for the phantom (see 3.3). The calibration procedure from the side of the end user would be as simple as attach the phantom to the holder on the UFASS (which would be designed that way that only one position is possible) and to start the calibration software. The rest would be performed automatically.

3.2. Results

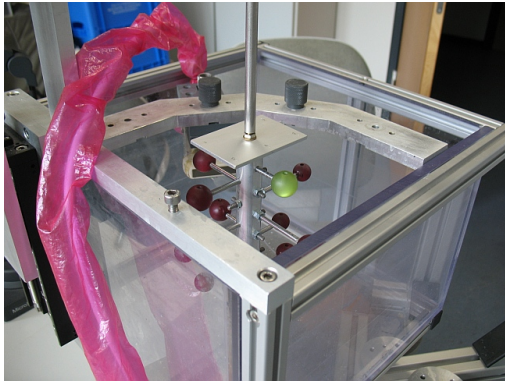
3.1.6 Application to other automatic scanners

We designed the multi-spheres phantom for the calibration of the UFASS according to its calibration objectives. However the phantom is flexible and may be also used for the calibration of other automated ultrasound scanners of similar construction. In our calibration method we make two assumptions about the ultrasound scanner. Firstly, the scanner should have a mechanical positioning system that supports precise probe movements with a small step within the defined trajectory. This feature is used during the "Data acquisition" calibration step. Secondly, there should be a possibility to measure the Scanner – Phantom transformation, either with an external device like described in our approach or using some built-in facilities of the scanner. This assumption is crucial on the "Scanner – Phantom transformation determination" step. If a scanner fulfils both of these requirements we can use the multi-spheres phantom for its calibration.

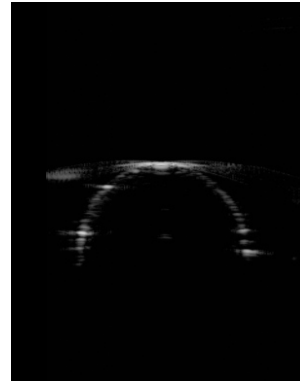
3.2 Results

According to the described calibration procedure we carried out ten calibration experiments. For each experiment the phantom coordinate system was measured independently. B-scans datasets were obtained with the 8 MHz linear transducer at 6 cm depth. For each collected dataset the calibration matrix was calculated twice – using both the CT and the Pointer models (see Section 3.1.4). The calibration error was calculated in terms of landmark points distance RMS between the model reference points and the US measured points. Average calibration error after 10 experiments was 0.42 mm RMS on the Pointer model and 0.6 on the CT model (see full results in the Table 3.5). The higher error on the CT model was caused by the unpreciseness of the model. Firstly, the CT scans in the Z-direction were taken with 0.6 mm step. Secondly, the phantom had a lot of metal parts which gave strong artefacts on the scans and complicated the detection of the landmarks which caused inaccuracy in the model data.

The presented calibration method and the multi-spheres phantom are developed to fulfil the objectives of the UFASS calibration (see Table 3.6). Current calibration procedure implementation with the UFASS prototype does not fully support two of the objectives – the "Execution simplicity and speed" and "Self-sufficiency and expert independence". The reason we rate it as partly fulfilled is the dependence of the calibration procedure on the Scanner – Phantom transformation determination. We have discussed that this step would be implemented automatically in the final scanner version, but on the prototype we have to perform the coordinate system measurement manually with the spatial localizer device. However the whole procedure is anyway very fast and easy and it takes less than a minute to perform the measurements. For example, in comparison



(a) Phantom attached to the UFASS



(b) B-scan of a ball

Figure 3.12: Multi-spheres phantom in the UFASS calibration.

to alignment phantoms, where very precise time-consuming alignment should be executed, our technique allows us to say that this requirements is partly fulfilled even in the prototype version.

The fulfilment of the calibration requirements for the UFASS is measured according to the following criteria:

- **Robustness.**

The phantom consists only from non-deformable parts, e.g. metal or solid plastic, preferably not thin wires. Can not be damaged by occasion, e.g. when hold too hard, but only by applying explicit force.

- **Low costs and construction simplicity.**

The material and production costs lie in the price segment under approx. 50 Euro. No special devices and no precise measurements are required for the phantom manufacturing.

- **Execution simplicity and speed.**

The calibration procedure consists of several easy steps without decision making, e.g. the user is not supposed to influence the calibration procedure, but performs simple steps like "fixate the phantom", "press the button", etc. The whole procedure takes no more than several minutes (up to five).

- **Self-sufficiency and expert-independence.**

No additional equipment (like extra position sensors) are required during the calibration. A user performing the procedure may have no experience with ultrasound calibration, and no additional expert is involved.

- **Distances range support.**

Minimum one of the phantom landmarks can be positioned in the US probe focus for at least a half of different transducer focal lengths. The focal length of the UFASS transducers are from 3 to 10 cm, that's why at least 4 different depth position must be supported.

3.2. Results

Experiment \ Model	CT	Pointer
1	0.6332	0.5522
2	0.7051	0.4163
3	0.5353	0.3571
4	0.5404	0.3203
5	0.6060	0.4867
6	0.5516	0.5539
7	0.7588	0.4328
8	0.5812	0.3171
9	0.4018	0.3258
10	0.6804	0.4748
mean RMS	0.5994	0.4237

Table 3.5: UFASS calibration RMS error (in mm) with the multi-spheres phantom.

- **Positions and orientations variety support.**

Minimum one of the landmarks can be scanned by both transducers from at least a half of possible transducer positions and orientations, that are 360 degree rotation around the scanner axis, and approx. 10 cm elevation in the vertical direction. It is meaningful to cover at least four rotations (north/south/east/west) and at least 5 elevation positions with 2 cm distances between them.

- **Automatic images processing.**

Phantom landmarks are automatically detected from the ultrasound images by a segmentation algorithm. No input or decision making is required from a user.

Since most of the criteria are non-measurable we do the evaluation with a true/false measure. The phantom satisfying a criterion gets a plus (+) in this category, not satisfying — a minus (-). In case of partial fulfillment we give a +/- note.

Chapter 3. The multi-spheres phantom for the UFASS calibration

UFASS calibration objectives	Multi-spheres	Multi-wires
Robustness	<p style="text-align: center;">+</p> <p>Stable construction with no movable parts, non-sensible to temperature variations, not easy to damage, easy to handle.</p>	<p style="text-align: center;">+</p> <p>No movable parts, easier to damage due to the presence of thin nylon wires, but still stable. Nylon may be deformed in hot water, however is stable to warm water that was used in our experiments.</p>
Low costs and construction simplicity	<p style="text-align: center;">+</p> <p>Consists of several cheap metal bars and plastic balls (costs appr. 15 Euro), for construction requires only simple equipment such as a manual milling device. May be easily produced with the 3D printer (that may even increase the accuracy due to the very accurate model).</p>	<p style="text-align: center;">+</p> <p>Consists of several cheap beads, nylon wires and metal planes (costs appr. 10 Euro), for construction requires only simple equipment such as a manual milling device.</p>
Execution simplicity and speed	<p style="text-align: center;">+/- [<i>For the prototype</i>]</p> <p>Half-automatic execution of the transducers movements because the prototype is not equipped with motors. The whole procedure takes around 10 Minutes.</p> <hr style="width: 20%; margin: 10px auto;"/> <p style="text-align: center;">+ [<i>For the final scanner</i>]</p> <p>Very easy calibration procedure, the user must only attach the phantom and start the calibration software. The whole procedure must take not more than a minute.</p>	<p style="text-align: center;">-</p> <p>Slow calibration time with manual alignment of the transducer with the beads and their manual segmentation on the images afterwards. The whole procedure takes around 20-30 minutes.</p>

3.2. Results

UFASS calibration objectives	Multi-spheres	Multi-wires
Self-sufficiency and expert-independence	<p>+/- [<i>For the prototype</i>] An additional measurement device (spatial localizer) is required to obtain the phantom position within the scanner. The procedure is easy and does not require special experience from a user.</p> <hr/> <p>+ [<i>For the final scanner</i>] No additional equipment other than provided with the UFASS is required. No experience from the end user.</p>	<p>-</p> <p>An additional measurement device (spatial localizer) is required to obtain the phantom position within the scanner. However the same phantom holder that is suggested for the multi-spheres phantom may be used for this phantom as well. Nevertheless the transducer alignment with the beads landmarks remains pure manual and requires a well-experienced user.</p>
Distances range support	<p>+</p> <p>Landmarks are positioned that way that they have a range of distances about 4cm, it means some landmarks are up to 4 cm farther than the others. It helps to calibrate the transducer more precise on different focal lengths or to variate the "detection accuracy - rotation angle" parameters.</p>	<p>-</p> <p>All wires with beads landmarks are located symmetrically around the main phantom axis with no distances range.</p>
Positions and orientations variety support	<p>+</p> <p>Landmarks are located on different heights and different rotation angles relatively to the phantom axis that covers the full motion trajectory for both UFASS transducers.</p>	<p>+</p> <p>Provides the same positions and orientations support as the multi-spheres transducer.</p>

UFASS calibration objectives	Multi-spheres	Multi-wires
Automatic images processing	+ Fully automated B-scan segmentation with spherical landmarks detection.	- Beads must be manually detected on the B-scans.

Table 3.6: Fulfilment of the UFASS calibration objectives by the multi-spheres and the multi-wires calibration phantoms.

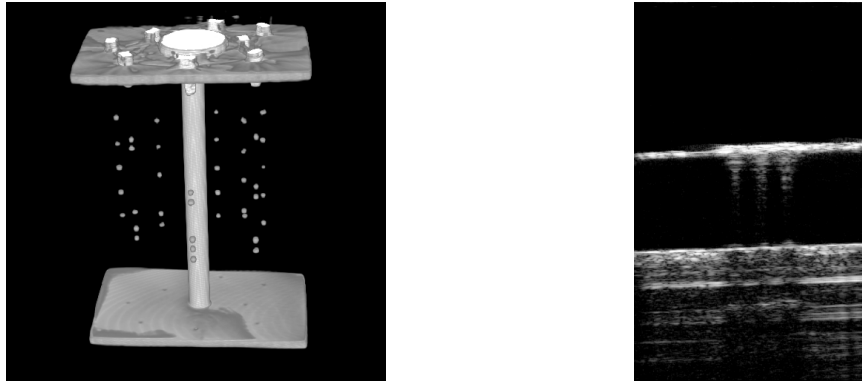
3.2.1 Alternative calibration with the multi-wires phantom

To evaluate our solution with the multi-spheres phantom we compared it to the calibration on another, multi-wires phantom which was originally designed for the UFASS (©UltraOsteon GmbH). We chose this phantom for comparison other than any state of the art phantoms from several reasons. Firstly, it belongs to the point phantoms class as well as the spheres phantom that makes the comparison easier and more fair. Secondly, as stated in the analysis of standard calibration phantoms, there are no solutions that satisfy the UFASS calibration requirements, and the point-phantom class has at most satisfactory characteristics for the UFASS. And finally, the multi-wires phantom is invented especially for the UFASS and optimized for its construction and calibration requirements.

The phantom has one central metal axis with two metal planes on the top and on the bottom of it. Between these two planes several thin nylon wires are stretched with small glass beads glued on them (see Fig. 3.13a). These beads are used as the point landmarks and should be captured with the scanner’s transducers. The top plane has coordinate system marks that are used to detect the phantom position within the UFASS, this procedure is similar to that one used for our multi-wires phantom. For the calibration procedure the phantom should be placed into the UFASS centre so that the beads are visible to both transducers from different positions and orientations.

We performed the calibration procedure with this phantom on the same settings that were used for the multi-spheres phantom. The calibration procedure was performed as follows. Firstly, the phantom model was obtained once before the calibration starts. It was a volume built with the *GE LightSpeed 16* CT scanner with 0.21875 x 0.21875 x 0.6 mm resolution where the landmark points were detected manually. For the calibration the phantom was fixed on a special holder and placed into the water-filled UFASS. Phantom location in the scanner

3.2. Results



(a) Phantom CT model (©UltraOsteon GmbH) (b) B-scan of a wire with three beads

Figure 3.13: Multi-wires phantom.

coordinate system was measured with the spacial localizer. For each of the beads the probe was manually aligned with the bead's centre by an operator. Then the landmarks' centres were manually detected on the B-scans. Reference landmark coordinates were taken from the model. Finally, US data points and model reference points were placed into the equation (1.1) and the calibration matrix was calculated with an optimization algorithm. The calibration procedure took around 25 minutes. We received the calibration error of 0.28 mm RMS which is very low. The calibration error reported by the phantom owner is even lower (0.15 mm RMS), the difference may be caused by different settings and the fact that manual operations are not repeatable and depend strongly on the expert's opinion and experience.

The low calibration error is of course the main advantage of this solution. The main disadvantage is the necessity for landmarks manual alignment and detection. The transducer should be operated by an expert who should carefully align it with the bead's centre. Afterwards each bead should be manually detected on the B-scan. Both are rather time-consuming procedures and influence the result accuracy strongly. In the Table 3.6 we rate the phantom properties according to the proposed objectives of the UFASS calibration.

3.3 Discussion

We presented the new multi-spheres phantom in application to the UFASS calibration. According to the phantom design the calibration procedure satisfies all of the UFASS calibration requirements and is fully automatic when performed on the clinical device. We achieved the main goal of the UFASS calibration – the automatic image processing – by using the sequential landmarks scanning algorithm with circle template matching to automatically detect the spheres centres in an images sequence. Moreover, this idea also provides the automatic data acquisition procedure, that is not achieved in any other standard calibration phantoms. The detailed description of the implementation for each calibration goal is provided in the "Results" section of this chapter.

Unfortunately the real clinical device was not available at the moment of experiments. We tested our calibration solution on the system prototype having only half-automatic transducer position controller, therefore the calibration procedure was slightly changed and was half-automatic. There are two modifications that differ the final scanner version from it's prototype. Firstly, transducers motion is performed not mechanically by the controller, but signals for each next step are given manually. Secondly, the "Scanner – Phantom transformation determination" step is done manually. In the prototype version we use an additional device, the spatial localizer, to obtain the coordinate system of the phantom.

For the tested prototype configuration the phantom satisfies two of the calibration requirements only partly. The "Self-sufficiency and expert-independence" objective is not fully satisfied because we use a spatial localizer device for the scanner positioning. The "Execution simplicity and speed" objective is partly fulfilled because calibration procedure duration with the half-automatic scanner is higher than is designed for the scanner equipped with automatic motion controllers. This result is however anyway better than for the other state of the art phantoms and the multi-wires phantom. The problem of determining the position of the phantom within the scanner exists for any type of the phantom, that's why no described state-of-the-art calibration solutions may outperformed the multi-spheres phantom by this criterion. Speed of the calibration can not be directly compared for all known phantoms because for the manual calibration it strongly depends on the experience of the user performing it. However we should only compare our solution with the phantoms with automatic image segmentation because it is the main objective for the UFASS calibration. The standard phantoms with automatic image processing are the single wall phantom, Cambridge phantom, the Mechanical Instrument from Gee et al., and the combined plane-wires phantom. The first and the last are not applicable for the UFASS calibration because they require the scans to be done only from one position – perpendicular to the plane surface – that does not satisfy the requirement of phantom visibility from different positions and orientations. The Cambridge phantom and the Mechan-

3.3. Discussion

ical Instrument are not applicable for the UFASS as explained in the Analysis section of this work. The outperformance of the standard calibration approaches is the main advantage of our multi-spheres phantom. The disadvantage is its lesser accuracy than the accuracy of the multi-wires phantom. Our calibration error is 0.42 mm RMS that is higher than the error of the multi-wires phantom. However it must be admitted that this difference is not significant, moreover the calibration error of the majority of calibration phantoms lies over 0.5 mm RMS which makes our phantom to a very accurate one.

To prove the full support of all of the UFASS calibration objectives the multi-spheres phantom must be tested on the fully-automated scanner other than on the prototype one. There are no potential difficulties that refer to the first prototype modification – deautomation of the transducer motion controller – because controller is fully simulated in the prototype version. The only difference is that each motion step is initiated not by a signal send by the computer to the controller but by a user pushing the correspondent button. Introducing the mechanical controller for this purpose in the clinical system should not involve any additional error.

The possible error-prone step of the calibration with the final clinical device may be the "Scanner – Phantom transformation determination" step. This is the only step that is significantly modified for usage with the prototype scanner in comparison to the initial calibration procedure. This step is done manually and consists in touching five points on the top of the phantom and five points on the top of the scanner with the tip of the localizer. Actually the procedure is easy and fast (around one minute), but anyway the calibration procedure is not fully automatic anymore, and an additional measuring device is required. Our proposal for automation of this step in the clinical scanner is to use a rigid phantom holder that allows to attach the phantom to the scanner in only one way. In this case the relation between the coordinate systems of the phantom and the scanner must be defined only once after the scanner construction when the holder is attached to it for the first time. The similar principle is used in [33]. This method should not provide any difficulties since the phantom and the scanner are very robust and such a holder, when designed solidly, can provide enough steadiness to keep the position unchanged. As an alternative this method can be replaced with one of the mostly commonly used – detection with the visual positioning camera. In this method visual markers, normally several small balls, should be attached to the phantom and to the scanner and a special camera should be positioned that way that all the markers are visible to it. The transformation matrix between both coordinate systems is then calculated automatically. This method is very precise and is used in many freehand ultrasound applications, but it's drawback is that we need an additional device – the positioning camera – for each clinical UFASS device.

Chapter 3. The multi-spheres phantom for the UFASS calibration

The calibration procedure on the prototype takes around 10 minutes. We estimate the whole calibration procedure on the clinical device to take around one minute. The estimation is based on our experiments and observations how fast the transducer may be moved in water without causing too much fluctuations that distort the ultrasound image.

Being designed especially for the the UFASS the multi-spheres phantom is rather flexible to be used also with other automated scanners. The state of the art calibration phantoms are mostly designed for the freehand ultrasound and are not optimised for the usage with the automated scanners as well as they do not use the advantages provided by the automated transducer motion. The multi-spheres phantom directly relies on this property of automated ultrasound systems and demands a motion controller that can move transducer on the predefined trajectory with a small step. It is necessary for the spheres centre detection procedure. Therefore the phantom provides the fully-automated alignment and image detection procedure which is a critical part in many calibration solutions. If an automated scanner has such a motion controller than most probably the multi-spheres phantom is suitable for its calibration because its design is in no way too specific and supports a big variety of scanning position and orientations.

Future investigation can be focused on the improvement of those calibration procedure parts that has been only tested on the prototype UFASS, primarily the Scanner – Phantom transformation determination. It may also be possible to improve the spheres centre detection on the ultrasound images.

Conclusion

Usage of 2D ultrasound transducers in 3D medical systems makes the calibration task to one of the essential steps of the US investigation procedure, significantly influencing the resulting 3D reconstruction quality. Each US scanner has its own requirements to the calibration procedure, therefore the calibration solution varies from system to system. In this work we presented a novel multi-spheres phantom with a calibration procedure designed and optimised for the Ultrasound Fracture Analysis Scanning System – the automated scanner for orthopaedics, which provides 3D diagnostic information for human extremities.

The use cases of the UFASS in clinical praxis require a small, cheap, robust and easy in use phantom with a fast automated calibration procedure that requires no special experience from the end user, no calibration specialists involvement and no additional equipment. The most important criterion is the automated image processing. The construction of the scanner makes also the visibility of the phantom from different positions and orientations to one of the important requirements. The detailed analysis of the state of the art calibration phantoms shows that there is no fully automated calibration procedure and no phantom satisfying these requirements. That's why we designed the novel multi-spheres phantom and a correspondent calibration procedure that are optimized for the UFASS calibration. It is called multi-spheres because it is based on the spherical landmarks that are very practical for automatic detection. Compared to standard calibration solutions our phantom can provide the higher level of automation having both automatic data acquisition and image segmentation. This is possible because the landmarks of our phantom do not require precise alignment that would be only possible under a user manual control. The scanned data is analysed on the image segmentation step where the required landmarks are selected from the scans by the calibration algorithm. The UFASS transducer motion controller is used for data acquisition to obtain these scans without user interaction.

The phantom is designed to fulfil all seven UFASS calibration objectives. Practically we can report the realization of five out of those seven, and partial fulfilment of the other two. This is caused by the fact that for our experiments we used not the clinical device, but the UFASS prototype and had to modify the designed calibration procedure correspondently. The clinical device was not

available at the moment of described research and that's why the prototype was taken, that is a simplified version of the scanner with no motors. The scanner prototype supports only half-automatic transducers motion and has no phantom holder. That causes the variations from the designed calibration procedure and therefore partial fulfilment of the calibration objectives. More details about these variations are provided in the Discussion section of this work. However, this is anyway the best result between other analysed phantoms. The final calibration error using our phantom was measured as 0.42 mm RMS which is low and absolutely suitable for the application the phantom is designed for. The error is higher than the calibration error with the multi-wires phantom, but our solution is easier to execute and has fully-automatic image detection, that means it is also much faster and requires no expert involvement.

This multi-spheres phantom successfully solves the task of the UFASS calibration. Moreover, as mentioned in the correspondent section of this work, the phantom may also be used for other automated ultrasound scanners with similar construction. According to the proposed calibration algorithm the scanner must have a transducer motion controller for US data acquisition that provides a sequence of US images with small distances between them. If an automated scanner has such controller than we can recommend our phantom for its calibration as a simple, precise and automatic solution.

Appendix A

Spatial localizer

For the research described in this paper we needed a precise instrument to measure objects and obtain their 3D coordinates. For this purpose we used a spatial localizer MicroScribe® *G2X 3D digitizer*. We successfully used it to build the phantom point model, and to determine the coordinate systems transformation between the phantom and the UFASS.

It is a compact, portable, contact-based measuring instrument that captures data points in the 3D space. The main part of it is a mechanical arm with a pen-like looking pointer at one end (see Fig. 3.14). The used model has 5 DOF and can access points up to 1270 mm maximal distance from the device base [63]. Accuracy stated by the manufacturer is ± 0.23 mm.

Before using the localizer we performed a precision test. When measuring points with the localizer it was supposed that result precision should increase when one point was measured several times and the average value was taken instead of taking the single measurement data. For this purpose we should have been able to derive the average point from a set of localizer's measurements. Therefore, it was necessary to know the measurements distribution law for averaging the values properly. Presumably we should have seen the Gaussian distribution, however it should have been proved explicitly since it was not stated in the device documentation. Taking a wrong average value could affect the result precision poorly.

To learn the MicroScribe digitizer's distribution function we held the following experiment. A metal surface with a tiny pinned dot on it was taken. This single point was measured with the localizer 100 times in three modes:

1. The pointer was placed onto the dot perpendicular to the surface and it wasn't moved during all the 100 measurements.
2. The pointer was located as in the first mode but was slightly rotated (without loss of contact) before each of the 100 measurement was taken.
3. Before each measurement was taken the pointer-surface contact was broken,



Figure 3.14: MicroScribe 3D digitizer ([63]).

different manipulations within each localizer’s joint were made. Then the pointer was placed back onto the same point.

The purpose of the experiment was to build statistics that describe the distribution and to point out the average value acquisition rule.

According to the experiment results on the three modes pointer movements did not imply additional measurements inaccuracy. Table 3.7 shows the coordinates variance of 100 measurements for each mode for X, Y, Z coordinates separately and for the 3D coordinate (measured as euclidean distance from the coordinate system centre).

Variance \ Mode	1	2	3
X	0.0091	0.0105	0.0089
Y	0.0050	0.0118	0.0107
Z	0.0057	0.0097	0.0061
3D	0.0049	0.0147	0.0100

Table 3.7: MicroScribe spatial localizer measurements precision. Coordinates (in mm) variance is given for each of the three experiments.

From the experiment we could claim that localizer's measurements have normal distribution (see Fig. 3.15 with the results for the third mode). The shapes of the cumulative distribution function and the probability density function were not perfect, which was caused by rather small amount of data, however they were similar to the normal distribution shapes. This implied that a simple mean value could be taken as an average point.

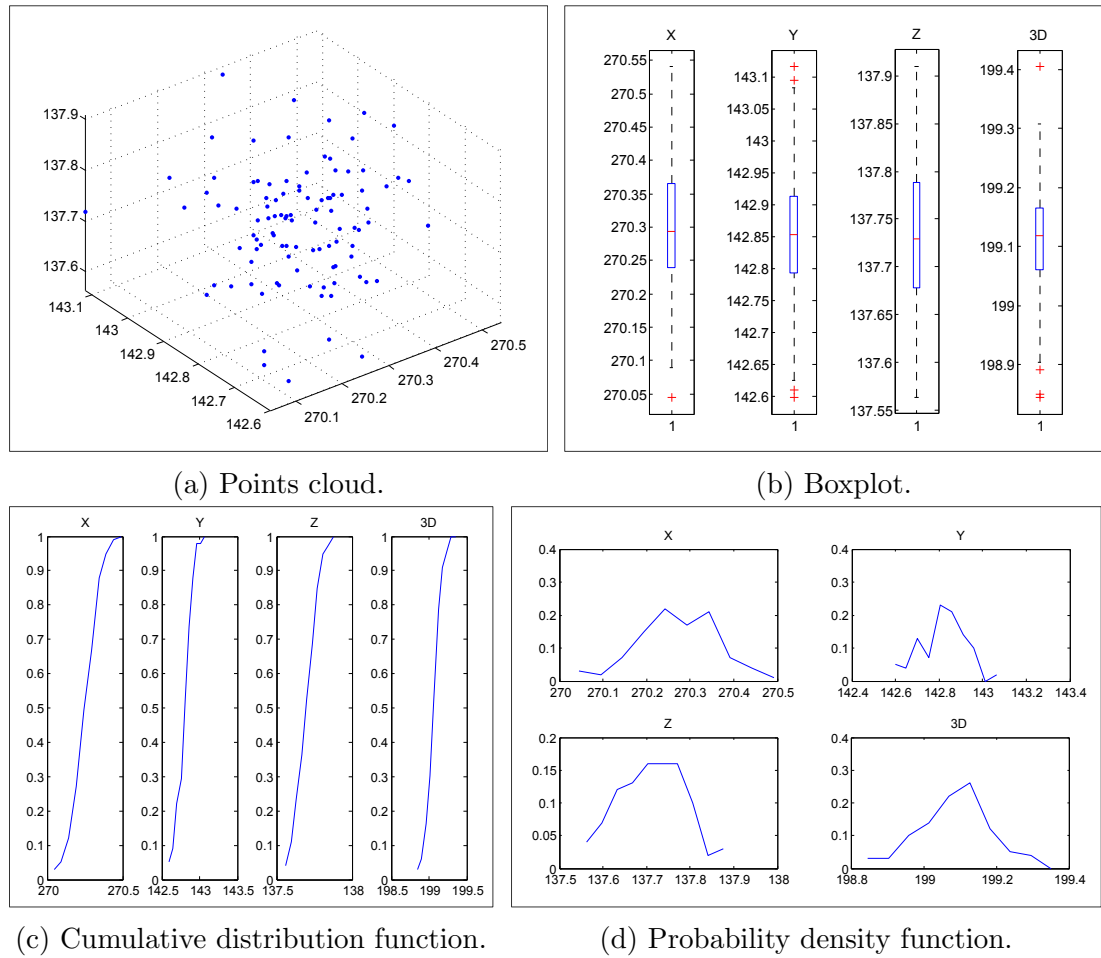


Figure 3.15: MicroScribe digitizer measurements precision.

Appendix B

Calibration software

For the calibration procedure with the multi-spheres phantom we provide the software executing all major operations. Current version is written in MatLab.

The software uses .conf files of the following format for storing points data, transformation matrices, image scaling and size:

```
[Transformation matrix section]
ImageTransform.Rot.x           = [0.939693 0.342020 0.000000]
ImageTransform.Rot.y           = [-0.342020 0.939693 0.000000]
ImageTransform.Rot.z           = [0.000000 0.000000 1.000000]
ImageTransform.Trans           = [0.000000 0.000000 52.000000]
SubImageInPixCosUL            = [0.000000 0.000000]
SubImageInPixCosUR            = [511.000000 511.000000]
ImageScaling                   = [0.115000 0.115000]

[Points data section]
contourPoint00003d            = [32.890000 53.130000 0.000000]
contourPoint00013d            = [31.280000 52.325000 0.000000]
contourPoint00023d            = [29.555000 51.750000 0.000000]
< ... >                       = < ... >
```

Figure 3.16: An example of the configuration file for the multi-spheres phantom calibration software.

The input data for the calibration procedure includes:

- A .conf file with the Phantom-Scanner transformation matrix.
- The folder with the ultrasound images and image transformation matrices stored each in a .conf file. The folder is organized as follows. Each sphere

is scanned several times and provides a series of scans with neighbourhood slices – for each such series there is one subfolder in the main data folder. For each image a .conf file containing the transformation with the same file name is stored together with the image.

- The phantom configuration .conf file. The file contains 3D coordinates of each phantom landmark in it's coordinate system, all together 12 points.
- The scanning plan file. It is a text file containing the sequence of numbers from 1 to 12 defining in what order the landmarks are scanned. Each number corresponds to one subfolder with sphere scans.

The output of the calibration procedure is a calibration matrix, which is stored in a .conf file, and the calibration error in terms of the rms of the distance between the phantom configuration points and the scanned ultrasound points reconstructed in 3D using the obtained calibration matrix.

Here is the pseudo-code of the main calibration procedure:

```
function calibrate()

% Define the 3D coordinates of landmark points correspondent to each
% phantom sphere (its centre), and the sizes of each sphere
phantom_configuration = load_phantom_configuration()

% Define the scanning plan - the order in that the landmarks are scanned
scanning_plan = load_scanning_plan()

% Get the transformation between the scanner and the phantom holder
get_scanner_phantom_transformation()

% Process input data from the ultrasound transducer. The data consists
% of images subsets, each subset for a sequence of scans for one sphere.
% For each image data also contains a transformation defining the position
% of this image in the scanner coordinate system.

data = load_data()
for each landmark_subset in data
    load images, transformations
    landmark_size = get_current_landmark_size(scanning_plan)
    for each image in images
        measure = detect_circle_on_the_image(landmark_size)
    end

    best_image = find_best_circle_measure(measures)
    landmark_point = circle_center(best_image)
    phantom_point = get_current_phantom_landmark(phantom_configuration)
```

```
    add_to_calibration_dataset(landmark_point, phantom_point,
                              current_transformation)
end

% Minimize the cost function between the phantom_points and the US
% landmark_points stored in the calibration_dataset
calibration_matrix = run_distance_minimization(calibration_dataset)

% Calculate the calibration error
calibration_error = rms(calibration_dataset, calibration_matrix)

end
```


Bibliography

- [1] Biochemical Micro System Engineering Laboratory, Department of Micro System Engineering, School of Engineering, Nagoya University, Japan. www.bmse.mech.nagoya-u.ac.jp/index-e.html. 42
- [2] J. M. Abeysekera and R. Rohling. Alignment and calibration of dual ultrasound transducers using a wedge phantom. *Ultrasound in Medicine and Biology*, 37(2):271–279, 2011. 38
- [3] A. Ali and R. Logeswaran. A visual probe localization and calibration system for cost-effective computer-aided 3D ultrasound. *Computers in Biology and Medicine*, 37(8):1141–1147, 2007. 21, 35
- [4] D. Amin, T. Kanade, B. Jaramaz, A. DiGioia, C. Nikou, R. LaBarca, and J. Moody. Calibration method for determining the physical location of the ultrasound image plane. In *Medical Image Computing and Computer-Assisted Intervention – MICCAI 2001*, volume 2208, pages 940–947. 2001. 26
- [5] A. Anagnostoudis and J. Jan. Cross-wire calibration for freehand 3D ultrasonography: Measurement and numerical issues. *Radioengineering*, 14(2):27–32, 2005. 20, 27
- [6] D. Atkinson, M. Burcher, J. Declerck, and J. A. Noble. Respiratory motion compensation for 3D freehand echocardiography. *Ultrasound in Medicine and Biology*, 27(12):1615–1620, 2001. 28
- [7] D. C. Barratt, A. H. Davies, A. D. Hughes, S. A. Thom, and K. N. Humphries. Accuracy of an electromagnetic three-dimensional ultrasound system for carotid artery imaging. *Ultrasound in Medicine and Biology*, 27(10):1421–1425, 2001. 20, 26
- [8] D. C. Barratt, G. P. Penney, C. S. K. Chan, M. Slomczykowski, T. J. Carter, P. J. Edwards, and D. J. Hawkes. Self-calibrating 3D-ultrasound-based bone registration for minimally invasive orthopedic surgery. *IEEE Transactions on Medical Imaging*, 25(3):312–323, 2006. 20, 26
- [9] C. D. Barry, C. P. Allott, N. W. John, P. M. Mellor, and P. A. Three-dimensional freehand ultrasound: Image reconstruction and volume analysis. *Ultrasound in Medicine and Biology*, 23(8):1209–1224, 1997. 20, 27

-
- [10] M. Baumann, V. Daanen, A. Leroy, and J. Troccaz. 3D-ultrasound probe calibration for computer-guided diagnosis and therapy. *CoRR*, abs/0801.3711, 2008. 21, 33
- [11] R. A. Beasley, J. D. Stefansic, A. J. Herline, L. Guttierrez, and R. L. Galloway. Registration of ultrasound images. In *Society of Photo-Optical Instrumentation Engineers (SPIE) Conference Series*, volume 3658, pages 125–132, 1999. 32
- [12] S. Berg, H. Torp, D. Martens, E. Steen, S. Samstad, I. Høivik, and B. Olstad. Dynamic three-dimensional freehand echocardiography using raw digital ultrasound data. *Ultrasound in Medicine and Biology*, 25(5):745–753, 1999. 21, 36
- [13] J. M. Blackall, D. Rueckert, C. R. Maurer Jr., G. P. Penney, D. L. G. Hill, and D. J. Hawkes. An image registration approach to automated calibration for freehand 3D ultrasound. In *MICCAI*, pages 462–471, 2000. 21, 39
- [14] F. Bludau, D. Hlindzich, P. Krasopevtsev, A. Kryvanos, U. Obertacke, and M. Schwarz. Ein neuartiger ansatz zur 3d-oberflachendarstellung von knochen mittels ultraschall. In *Meeting Abstract: Deutscher Kongress fuer Orthopaedie und Unfallchirurgie, DKOU11*, Oct 2011. 20, 43
- [15] E. Boctor, A. Viswanathan, M. A. Choti, R. H. Taylor, G. Fichtinger, and G. D. Hager. A novel closed form solution for ultrasound calibration. In *ISBI*, pages 527–530, 2004. 32
- [16] E. M. Boctor, A. Jain, M. A. Choti, R. H. Taylor, and G. Fichtinger. A rapid calibration method for registration and 3D tracking of ultrasound images using spatial localizer. In *Proceedings of SPIE: Ultrasonic Imaging and Signal Processing*, volume 5035, pages 521–532, 2003. 32
- [17] J. Boese, E. Camus, and M. John. Robotically assisted medical ultrasound. Patent, Jan 2012. US 2009/0326373 (A1). 42
- [18] B. Brendel, S. Winter, and H. Ermert. A simple and accurate calibration method for 3D freehand ultrasound. In *Biomedizinische Technik*, volume 49, pages 872–873. 2004. 28
- [19] J. Carr. *Surface Reconstruction in 3D Medical Imaging*. PhD thesis, University of Canterbury, 1996. 20, 30
- [20] T. K. Chen, P. Abolmaesumi, D. R. Pichora, and R. E. Ellis. A system for ultrasound-guided computer-assisted orthopaedic surgery. *Computer Aided Surgery*, 10(5-6):281–292, 2005. 32
- [21] T. K. Chen, A. D. Thurston, R. E. Ellis, and P. Abolmaesumi. A real-time free-hand ultrasound calibration system with automatic accuracy feedback and control. *Ultrasound in Medicine and Biology*, 35(1):79–93, 2009. 32
- [22] P. Cinquin, E. Bainville, and C. Barbe. Computer assisted medical interventions. *IEEE Eng Med Biol Magazine*, 14:254–263, 1995. 19

Bibliography

- [23] R. M. Comeau, A. Fenster, and T. M. Peters. Integrated MR and ultrasound imaging for improved image guidance in neurosurgery. In *Society of Photo-Optical Instrumentation Engineers (SPIE) Conference Series*, volume 3338, pages 747–754, 1998. 31, 32
- [24] R. M. Comeau, A. F. Sadikot, A. Fenster, and T. M. Peters. Intraoperative ultrasound for guidance and tissue shift correction in image-guided neurosurgery. *Medical Physics*, 27(4):787–800, 2000. 32
- [25] S. Dandekar, Y. Li, J. Molloy, and J. Hossack. A phantom with reduced complexity for spatial 3-D ultrasound calibration. *Ultrasound in Medicine and Biology*, 31(8):1083–1093, 2005. 33
- [26] C. Delgorge, F. Courreges, L. A. Bassit, C. Novales, C. Rosenberger, N. Smith-Guerin, C. Bru, R. Gilabert, M. Vannoni, G. Poisson, and P. Vieyres. A tele-operated mobile ultrasound scanner using a light-weight robot. *IEEE Transactions on Information Technology in Biomedicine*, 9(1):50–58, 2005. 42
- [27] P. R. Detmer, G. Bashein, T. Hodges, K. W. Beach, R. P. Filer, D. H. Burns, and D. E. Strandness Jr. 3D ultrasonic image feature localization based on magnetic scanhead tracking: In vitro calibration and validation. *Ultrasound in Medicine and Biology*, 20(9):923–936, 1994. 20, 27
- [28] A. Dubouski, A. Belevich, and O. Krivonos. Automating freehand ultrasound calibration using a plane phantom. In *PRIP*, pages 81–82, 2007. 35, 51
- [29] N. Duric, P. Littrup, L. Poulou, A. Babkin, R. Pevzner, E. Holsapple, O. Rama, and C. Glide. Detection of breast cancer with ultrasound tomography: First results with the Computed Ultrasound Risk Evaluation (CURE) prototype. *Med. Phys.*, 34(2):773–785, 2007. 43
- [30] M. K. Feldman, S. Katyal, and M. S. Blackwood. Us artifacts. *Radiographics*, 29(4):1179–1189, 2009. 41
- [31] GABIE. Active Guidance Based on Echographic Images. Joint project between LIRMM, (Montpellier) LRP (Paris), TIMC (Grenoble), CEA/SRSI (Fontenay-aux-Roses), Pitié Salpêtrière hospital (Paris) and Grenoble hospital. 42
- [32] S. A. Garawi, F. Courreges, R. S. H. Istepanian, and P. Gosset H. Zisimopoulos. Performance analysis of a compact robotic tele-echography E-Health system over terrestrial and mobile communication links. In *Fifth IEEE International Conference on 3G Mobile Communication Technologies*, 2004. 42
- [33] A. H. Gee, N. E. Houghton, G. M. Treece, and R. W. Prager. A mechanical instrument for 3D ultrasound probe calibration. *Ultrasound in Medicine and Biology*, 31(4):505–518, 2005. 21, 36, 38, 83

-
- [34] H. Gemmeke and N. V. Ruiter. 3D ultrasound computer tomography for medical imaging. *Nuclear Instruments and Methods in Physics Research Section A: Accelerators, Spectrometers, Detectors and Associated Equipment*, 580(2):1057–1065, 2007. 15, 42, 43
- [35] C. K. Glide-Hurst, N. Duric, and P. Littrup. Volumetric breast density evaluation from ultrasound tomography images. *Med. Phys.*, 35(9):3988–3997, 2008. 43
- [36] D. Gobbi, R. M. Comeau, and T. M. Peters. Ultrasound probe tracking for real-time ultrasound/MRI overlay and visualization of brain shift. In *Medical Image Computing and Computer-Assisted Intervention – MICCAI’99*, pages 920–927, 1999. 31, 32
- [37] M. J. Gooding, S. H. Kennedy, and J. Alison Noble. Temporal calibration of free-hand three-dimensional ultrasound using image alignment. *Ultrasound in Medicine and Biology*, 31(7):919–927, 2005. 28, 29
- [38] L. Gumb, J. Vagner, and N. Ruiter. Vorrichtung für eine ultraschallgestützte Computertomographie mit erweitertem Messbereich. Patent, Nov 2010. EP2253274. 42
- [39] P. V. C. Hough. Machine analysis bubble chamber pictures. In *Conference on High Energy Accelerators and Instrumentation*, pages 554–556, 1959. 28
- [40] P. W. Hsu, R. W. Prager, A. H. Gee, and G. M. Treece. Real-time freehand 3D ultrasound calibration. *Ultrasound in Medicine and Biology*, 34(2):239–251, 2008. 31, 32
- [41] P. W. Hsu, R. W. Prager, A. H. Gee, and G. M. Treece. Freehand 3D ultrasound calibration: A review. In *Advanced Imaging in Biology and Medicine*, pages 47–84. 2009. 19, 20, 26, 30, 34
- [42] P. W. Hsu, G. M. Treece, R. W. Prager, N. E. Houghton, and A. H. Gee. Comparison of freehand 3-D ultrasound calibration techniques using a stylus. *Ultrasound in Medicine and Biology*, 34(10):1610–1621, 2008. 29
- [43] Q. H. Huang, Y. P. Zheng, M. H. Lu, and Z. R. Chi. Development of a portable 3D ultrasound imaging system for musculoskeletal tissues. *Ultrasonics*, 43(3):153–163, 2005. 20, 27
- [44] X. Huang, L. F. Gutierrez, D. Stanton, P. C. W. Kim, and A. Jain. Image registration based 3D TEE-EM calibration. In *2010 IEEE International Symposium on Biomedical Imaging: From Nano to Macro*, pages 1209–1212, 2010. 21, 40, 51
- [45] J. Hung, R. Lang, F. Flachskampf, S. K. Shernan, M. L. McCulloch, D. B. Adams, J. Thomas, M. Vannan, and T. Ryan. 3d echocardiography: A review of the current status and future directions. *Journal of the American Society of Echocardiography*, 20(3):213–233, 2007. 23

Bibliography

- [46] W. Igl. Mechanical accessory for commercially available compound apparatuses for echo mammography. Patent, Dec 1984. US4485819. 42
- [47] Craig J. J. *Introduction to robotics: mechanics and control*. Addison-Wesley Pub Co, 1986. 25
- [48] S. Keitel, U. Mueller, and S. Schulz. Automatic ultrasonic testing method of spot welds in mass production of sheet metal goods, especially motor vehicle bodywork, whereby a program controlled robot arm is used to move and position an ultrasonic test head. Patent, Mar 2003. DE10125782. 42
- [49] A. Khamene, S. Vogt, F. Azar, T. Sielhorst, F. Sauer, and H. Niemann. Local 3D reconstruction and augmented reality visualization of free-hand ultrasound for needle biopsy procedures. *Medical Image Computing and Computer-Assisted Intervention - MICCAI 2003*, 2879:344–355, 2003. 28
- [50] A. Krupa. Automatic calibration of a robotized 3D ultrasound imaging system by visual servoing. In *ICRA 2006. Proceedings 2006 IEEE International Conference on Robotics and Automation, 2006*, pages 4136–4141, 2006. 27
- [51] T. Langø. *Ultrasound guided surgery: image processing and navigation*. PhD thesis, Norwegian University of Science and Technology, Faculty of Information Technology, Mathematics and Electrical Engineering, 2000. 21, 33
- [52] T. Lange and S. Eulenstein. Calibration of swept-volume 3D ultrasound. *EXP. PSYCHOL. APPLIED S*, 3:339–360, 1999. 21, 40
- [53] M. E. Legget, D. F. Leotta, E. L. Bolson, J. A. McDonald, R. W. Martin, X. N. Li, C. M. Otto, and F. H. Sheehan. System for quantitative three-dimensional echocardiography of the left ventricle based on a magnetic-field position and orientation sensing system. *IEEE Transactions on Biomedical Engineering*, 45(4):494–504, 1998. 20, 26
- [54] D. F. Leotta. An efficient calibration method for freehand 3-D ultrasound imaging systems. *Ultrasound in Medicine and Biology*, 30(7):999–1008, 2004. 21, 37
- [55] D. F. Leotta, P. R. Detmer, and R. W. Martin. Performance of a miniature magnetic position sensor for three-dimensional ultrasound imaging. *Ultrasound in Medicine and Biology*, 23(4):597–609, 1997. 20, 26
- [56] C. Li, L. Huang, N. Duric, H. Zhang, and C. Rowe. An improved automatic time-of-flight picker for medical ultrasound tomography. *Ultrasonics*, 49(1):61–72, 2009. 43
- [57] F. Lindseth, T. Langø, J. Bang, and T. A. Nagelhus Hernes. Accuracy evaluation of a 3D ultrasound-based neuronavigation system. *Computer Aided Surgery*, 7(4):197–222, 2002. 27

- [58] F. Lindseth, G. A. Tangen, T. Langø, and J. Bang. Probe calibration for freehand 3-D ultrasound. *Ultrasound in Medicine and Biology*, 29(11):1607–1623, 2003. 26, 27, 32
- [59] J. Liu, X. Gao, Z. Zhang, S. Gao, and J. Zhou. A new calibration method in 3D ultrasonic imaging system. In *Engineering in Medicine and Biology Society, 1998. Proceedings of the 20th Annual International Conference of the IEEE*, volume 2, pages 839–841, 1998. 32
- [60] S. Meairs, J. Beyer, and M. Hennerici. Reconstruction and visualization of irregularly sampled three- and four-dimensional ultrasound data for cerebrovascular applications. *Ultrasound in Medicine and Biology*, 26(2):263–272, 2000. 20, 27
- [61] L. Mercier, T. Langø, F. Lindseth, and D. L. Collins. A review of calibration techniques for freehand 3-D ultrasound systems. *Ultrasound in Medicine and Biology*, 31(4):449–471, 2005. 19, 21, 25, 26, 32
- [62] K. Meyer and F.A. Biocca. A survey of position trackers. *Teleoperators and virtual environments*, 1:173–200, 1992. 19
- [63] MicroScribe®. 3D Digitizer (CMM) Product Details. http://microscribe.ghost3d.com/gt_microscribe.htm. 16, 87, 88
- [64] D. M. Muratore and R. L. Galloway Jr. Beam calibration without a phantom for creating a 3-D freehand ultrasound system. *Ultrasound in Medicine and Biology*, 27(11):1557–1566, 2001. 29
- [65] M. Najafi, N. Afsham, P. Abolmaesumi, and R. Rohling. Single wall closed-form differential ultrasound calibration. In *Proc. of SPIE Medical Imaging Conference*, 2012. 21, 33
- [66] OTELO. Mobile tele-echography using an ultra-light robot. EU project, Contract Number: IST-2001-32516. 15, 42
- [67] N. Pagoulatos, W.S. Edwards, D.R. Haynor, and Y. Kim. Interactive 3D registration of ultrasound and magnetic resonance images based on a magnetic position sensor. *IEEE Transactions on Information Technology in Biomedicine*, 3(4):278–288, 1999. 20, 26
- [68] N. Pagoulatos, D. R. Haynor, and Y. Kim. A fast calibration method for 3-D tracking of ultrasound images using a spatial localizer. *Ultrasound in Medicine and Biology*, 27(9):1219–1229, 2001. 31, 32
- [69] M. Peterhans, H. Talib, M. G. Linguraru, M. Styner, and M. A. G. Ballester. A method for frame-by-frame US to CT registration in a joint calibration and registration framework. In *5th IEEE International Symposium on Biomedical Imaging: From Nano to Macro, 2008. ISBI 2008*, pages 1131–1134, 2008. 21, 40

Bibliography

- [70] F. Pierrot, E. Dombre, E. Dégoulange, L. Urbain, P. Caron, S. Boudet, J. Gariépy, and J. L. Mégnien. Hippocrate: a safe robot arm for medical applications with force feedback. *Medical Image Analysis*, 3(3):285–300, 1999. 42, 43
- [71] C. T. Poon and R. N. Rohling. Comparison of calibration methods for spatial tracking of a 3D ultrasound probe. *Ultrasound in Medicine and Biology*, 31(8):1095–1108, 2005. 29, 32, 33
- [72] R. W. Prager. Ultrasound machine calibration. Patent, Aug 1997. GB9716994.0. 21, 34
- [73] R. W. Prager, R. N. Rohling, A. H. Gee, and L. Berman. Rapid calibration for 3-D freehand ultrasound. *Ultrasound in Medicine and Biology*, 24(6):855–869, 1998. 15, 19, 20, 21, 25, 28, 30, 33, 34
- [74] F. Rousseau, P. Hellier, and C. Barillot. Confusius: A robust and fully automatic calibration method for 3D freehand ultrasound. *Medical Image Analysis*, 9(1):25–38, 2005. 21, 33
- [75] Siemens ACUSON S2000ABVS. Das Ultraschallgerät für die automatische Erstellung räumlicher Ultraschallaufnahmen der Brust. <http://www.medical.siemens.com/webapp/wcs/stores/servlet/ProductDisplay?catalogId=-3&catTree=100000&langId=-3&productId=187041&storeId=10001>. 42
- [76] S. E. Salcudean, G. S. Bell, P. D. Lawrence, A. Marko, and M. Jameson. Robotically assisted medical ultrasound. Patent, Jul 2002. US6425865 (B1). 42
- [77] S. E. Salcudean, W. H. Zhu, P. Abolmaesumi, S. Bachmann, and P. D. Lawrence. A robot system for medical ultrasound. In *9th International Symposium of Robotics Research (ISRR'99), Snowbird*, pages 152–159, 1999. 42
- [78] Y. Sato, M. Nakamoto, Y. Tamaki, T. Sasama, I. Sakita, Y. Nakajima, M. Monden, and S. Tamura. Image guidance of breast cancer surgery using 3-D ultrasound images and augmented reality visualization. *IEEE Transactions on Medical Imaging*, 17(5):681–693, 1998. 21, 36
- [79] F. Sauer, A. Khamene, B. Bascle, L. Schinunang, F. Wenzel, and S. Vogt. Augmented reality visualization of ultrasound images: system description, calibration, and features. In *Proceedings of IEEE and ACM International Symposium on Augmented Reality, 2001*, pages 30–39, 2001. 28
- [80] R. E. N. Shehada. Scanning devices for three-dimensional ultrasound mammography. Patent, Sep 2007. US7264592. 42
- [81] A. State, D. T. Chen, C. Tector, A. Brandt, H. Chen, R. Ohbuchi, M. Bajura, and H. Fuchs. Case study: Observing a volume rendered fetus within a pregnant patient. In *Proceedings of the 1994 IEEE Visualization Conference*, pages 364–368, 1994. 20, 26

- [82] G. M. Treece, A. H. Gee, R. W. Prager, C. J. C. Cash, and L. H. Berman. High-definition freehand 3-D ultrasound. *Ultrasound in Medicine and Biology*, 29(4):529–546, 2003. 28
- [83] J. W. Trobaugh, W. D. Richard, K. R. Smith, and R. D. Bucholz. Frameless stereotactic ultrasonography: method and applications. *Computerized Medical Imaging and Graphics*, 18(4):235–246, 1994. 20, 27
- [84] J. Varandas, P. Baptista, J. Santos, R. Martins, and J. Dias. Volus—a visualization system for 3D ultrasound data. *Ultrasonics*, 42(1–9):689–694, 2004. 21, 35
- [85] A. Vilchis, K. Masuda, J. Troccaz, and P. Cinquin. Robot-based tele-echography: the TER system. *Stud Health Technol Inform*, 95:212–217, 2003. 42
- [86] J. Wang, T. Wang, L. Hu, H. Liao, K. Luan, and I. Sakuma. A fully automatic 2D ultrasound probe calibration method using a simple phantom. In *2011 4th International Conference on Biomedical Engineering and Informatics (BMEI)*, volume 2, pages 588–592, 2011. 28
- [87] J. N. Welch, J. A. Johnson, M. R. Bax, R. Badr, and R. Shahidi. A real-time freehand 3D ultrasound system for image-guided surgery. In *Ultrasonics Symposium, 2000 IEEE*, volume 2, pages 1601–1604, 2000. 21, 36
- [88] H. Yashiki. Automatic ultrasonic inspection device, inspection method and manufacturing method using its inspection method. Patent, Aug 2006. JP2006220608. 42
- [89] H. Zhang, F. Banovac, A. White, and K. Cleary. Freehand 3D ultrasound calibration using an electromagnetically tracked needle. In *Proceedings of SPIE: Visualization, Image-Guided Procedures, and Display*, volume 6141, pages 775–783, 2006. 20, 26
- [90] W. Y. Zhang, R. N. Rohling, and D. K. Pai. Surface extraction with a three-dimensional freehand ultrasound system. *Ultrasound in Medicine and Biology*, 30(11):1461–1473, 2004. 31, 32
- [91] W. H. Zhu, S. E. Salcudean, S. Bachmann, and P. Abolmaesumi. Motion/force/image control of a diagnostic ultrasound robot. In *IEEE International Conference on Robotics and Automation, 2000. Proceedings. ICRA '00*, volume 2, pages 1580–1585, 2000. 42

Acknowledgements

This thesis presents the results of the work that I have done at the Institute for Computer Engineering, Heidelberg University, Germany.

First of all I would like to thank Prof. Dr. Reinhard Männer for his continuous support and thorough guidance during my work.

My particular thanks to Prof. Dr. Jürgen Hesser for his great assistance, important remarks improving the quality of this work, and a lot of advice.

I would like to thank Dr. Aleh Kryvanos for our collaboration, fruitful discussions and his valuable ideas. This work could not be possible without his exceptional contribution.

I am also grateful to my colleagues in the Institute for Computer Engineering and the University Medical Center Mannheim for the pleasant working environment and productive cooperation.

Alena Bakulina

Mannheim, September 2015